GAZİ ÜNİVERSİTESİ

Gazi

1926

INVESTIGATION OF ELECTRONIC AND OPTICAL PROPERTIES OF WURTZITE MgZnO WITH FIRST PRINCIPLES CALCULATIONS

A THESIS SUBMITTED TO

THE GRADUATE SCHOOL OF NATURAL AND APPLIED SCIENCES

OF

GAZİ UNIVERSITY

BY

Rokaia IBRAHEM

IN PARTIAL FULFILLMENT OF THE REQUIREMENTS

FOR

THE DEGREE OF MASTER OF SCIENCE

IN PHYSICS

SEPTEMBER 2018

The thesis study titled "INVESTIGATION OF ELECTRONIC AND OPTICAL PROPERTIES OF WURTZITE MgZnO WITH FIRST PRINCIPLES CALCULATIONS" is submitted by Rokaia IBRAHEM in partial fulfillment of the requirements for the degree of Master of Science in the Department of Physics, Gazi University by the following committee.

Supervisor: Prof. Dr. Sefer Bora LİŞESİVDİN

Physics Department, Gazi University

I certify that this thesis is a graduate thesis in terms of quality and content   …..………..…………..

Chairman: Assoc. Prof. Dr. Özlem DUYAR COŞKUN

Physics Engineering Department, Gazi University

I certify that this thesis is a graduate thesis in terms of quality and content   …..………..…………..

Member: Prof. Dr. Mehmet KASAP

Physics Department, Gazi University

I certify that this thesis is a graduate thesis in terms of quality and content   …..………..…………..

Date: 21/9/2018

I certify that this thesis, accepted by the committee, meets the requirements for being a Master of Science Thesis.

…………………….…….

Prof. Dr. Sena YAŞYERLİ

Director of Graduate School of Natural and Applied Sciences

ETHICAL STATEMENT

I hereby declare that in this thesis study I prepared in accordance with thesis writing rules of Gazi University Graduate School of Natural and Applied Sciences;

- All data, information and documents presented in this thesis have been obtained within the scope of academic rules and ethical conduct,

- All information, documents, assessments and results have been presented in accordance with scientific ethical conduct and moral rules,

- All material used in this thesis that are not original to this work have been fully cited and referenced,

- No change has been made in the data used,

- The work presented in this thesis is original,

or else, I admit all loss of rights to be incurred against me.

<div align="right">

Rokaia IBRAHEM

21/09/2018

</div>

INVESTIGATION OF ELECTRONIC AND OPTICAL PROPERTIES OF WURTZITE

MgZnO WITH FIRST PRINCIPLES CALCULATIONS

(M.Sc. Thesis)

Rokaia IBRAHEM

GAZİ UNIVERSITY

THE GRADUATE SCHOOL OF NATURAL AND APPLIED SCIENCES

September 2018

ABSTRACT

In this study, the electronic and the optical properties of wz-ZnO and wz- $Mg_xZn_{1-x}O$ have been calculated for different Mg mole fractions using the Atomistic Toolkit-Virtual Nano Lab (ATK-VNL) software based on density functional theory (DFT). Our calculations are performed using the hybrid-generalized gradient approximation (GGA+U) formalism, where the Hubbard parameters are applied to Zn-3d electrons and O-2p electrons. The electronic properties calculations include the electronic band structures, the density of states and electron effective masses, whereas the optical properties calculations include the static dielectric functions, refractive indexes, extinction coefficients and absorption spectra of all the studied structures. The results show that the band gap energies increase as the Mg mole fractions increase, which corresponds with the previous experimental results. The electron effective masses calculation shows a linear dependence of the Mg mole fraction, but their values show overestimation. The absorption edges of studied structures move toward the higher energies region (the lower wavelengths region) as Mg mole fraction of $Mg_xZn_{1-x}O$ increases. The static dielectric constant of $Mg_xZn_{1-x}O$ decreases as Mg mole fraction increases. The dielectric constants of the high frequency of $Mg_xZn_{1-x}O$ are found to be very similar to the experimental results. In addition, the refractive indexes and the extinction coefficients move toward the higher energy region (the lower wavelength region).

HEKZAGONAL MgZnO KRİSTALİNİN ELEKTRONİK VE OPTİK
ÖZELLİKLERİNİN İLK PRENSİPLER HESAPLAMALARI İLE İNCELENMESİ
(Yüksek Lisans Tezi)

Rokaia IBRAHEM

GAZİ ÜNİVERSİTESİ
FEN BİLİMLERİ ENSTİTÜSÜ
Eylül 2018

ÖZET

Bu çalışmada, hekzagonal ZnO ve farklı Magnezyum (Mg) alaşım oranlarına sahip $Mg_xZn_{1-x}O$ yapıların elektronik ve optik özellikleri yoğunluk fonksiyonel teorisi (DFT) temelli Atomistix Toolkit-Virtual NanoLab (ATK-VNL) yazılımı kullanılarak gerçekleştirilmiştir. Hesaplamalarımız, ZnO kristalinde Zn atomunun 3d ve O atomunun 2p orbitallerine Hubbard (U) parametreleri uygulanıp Genelleştirilmiş Gradyent Yaklaşımı (GGA+U) kullanılarak gerçekleştirilmiştir. Tüm incelenen yapılar için elektronik bant yapısı, durum yoğunluğu (DOS) ve elektron etkin kütlesi gibi elektronik özelliklerin yanı sıra yapıların dielektrik fonksiyonu, kırılma indisi, sönüm katsayısı ve soğurma spektrumu gibi optik özellikleri incelenmiştir. Artan Mg alaşım oranına bağlı olarak $Mg_xZn_{1-x}O$ kristalinin yasak bant aralığının arttığı ve deneysel sonuçlara benzer olduğu görülmüştür. Mg alaşım oranına bağlı olarak elektron etkin kütlesi doğrusal olarak artış göstermektedir. Hesaplanan etkin kütle değerleri deneysel sonuçlarla kıyaslandığında benzer sonuçlar sergilemiştir. $Mg_xZn_{1-x}O$ kristalinin Mg oranı arttıkça kristalin soğurma kıyısı yüksek enerji bölgelerine (düşük dalga boyları) doğru kaymıştır. İncelenen yapıların statik dielektrik sabitleri artan Mg oranına bağlı olarak azalmıştır. Yüksek frekans dielektrik sabiti deneysel sonuçlara çok yakın olarak bulunmuştur. Ayrıca incelenen yapılar için kırılma indisleri belirlenmiştir.

ACKNOWLEDGEMENTS

TABLE OF CONTENTS

LIST OF TABLES

LIST OF FIGURES

Figures   **Pages**

LIST OF SYMBOLS AND ABBREVIATIONS

The symbols and abbreviations used in this thesis are presented in below with explanations.

Symbols	Explanations
$\hat{E}$	Total energy opertor
$\hat{H}$	Hamiltonian opertor
$\hat{T}$	Kinetic energy
c/a	Ratio between the lattice parameters
C_{ij}	Stiffness constant
$E_{ex}[n]$	Exchange-correlation functional
E_F	Fermi level
E_g	Band gap energy
E_U	Orbital-dependent term
$E_v[n]$	Energy functional
$E_{xc}[n]$	Exchange energy functional
$F_{HK}[n]$	Hohenberg-Kohn functional
k	Extinction coefficient
m_e	Electron effective mass
n	Refractive index
T[n]	Kinetic energy functional
u	Internal parameter
U[n]	Electron-electron interaction functional
V_{ee}	Coulomb effects between the electrons
V_{ext}	External forces on the electrons
α	Absorption coefficient
α, β	Bond angles
ε	Dielectric constant
ε(0)	Static dielectric constant
ε(∞)	High frequency of dielectric constant
$ε_1$	Real part of dielectric constant
$ε_2$	Imaginary part of dielectric constant

Symbols	Explanations
ε_r	Complex dielectric constant
λ	Wave length

Abbreviations	Explanations
ATK-VNL	Atomistic toolkit-virtual Nano lab
CBM	Conduction band minimum
CdO	Cadmium oxide
CVD	Chemical vapor deposition
DFT	Density functional theory
GaN	Gallium nitride
GEA	Gradient expansions approximation
GGA	Generalized gradient approximation
GGA+U	Generalized gradient approximation plus Hubbard parameter
hcp	Hexagonal close pocked
HF-SCF	Hartree-Fock self-consistent field
LCAO	Linear combination of atomic orbitals
LDA	Local density approximation
LDA+U	Local density approximation plus Hubbard parameter
Meta+GGA	Meta generalized gradient approximation
MgO	Magnesium oxide
MgZnO	Magnesium zinc oxide
OPW	Orthogonalized plane-wave method
PECVD	Plasma-enhanced chemical vapor deposition
rs-MgZnO	Rock-salt magnesium zinc oxide
rs-ZnO	Rock-salt zinc oxide
TCOs	Transparent conducting semiconductor
VBM	Valence band maximum
wz-MgZnO	Wurtzite magnesium zinc oxide
wz-ZnO	Wurtzite zinc oxide
zb-ZnO	Zinc blende zinc oxide
ZnO	Zinc Oxide

1. INTRODUCTION

The semiconductors are very important materials that caused the technical revolution because of their versatile applications in our life, in particular, II-VI semiconductors that we can use in industries. Zinc oxide (ZnO) is such an example. ZnO material received a special attention from both experimental and theoretical investigation because of its electronic, optical and piezoelectric properties such as a huge binding energy for free-exciton (60 meV) at 300K, a wide and direct forbidden gap (3.37 eV) in the NUV spectral region, a huge piezoelectric coefficient, a strong luminescence, a high thermal conductivity, a high electron mobility, a transparency in the visible region and its radiation hardness. In addition, ZnO is non-toxic, economic and environmentally safe material. ZnO can make alloys or heterostructures with magnesium oxide (MgO) and/or cadmium oxide (CdO), but ZnO has a wurtzite structure whereas Mg and CdO have the rock-salt structure where phase separation is expected to happen. So, the ZnO make alloy until the moderate concentration of MgO (until 37 %) where magnesium zinc oxide (MgZnO) alloys have the wurtzite crystal structure of ZnO with a wide range of band gaps (3.37– 4.0 eV). All these properties make ZnO a very suitable material for manufacturing short wavelength optoelectronic devices [1-5].

In the last decade, a lot of theoretical investigations that have relied on density functional theory studied the properties of ZnO. In these investigations, generalized-gradient approximation (GGA) and the local-density approximation (LDA) were used to calculate the electronic and optical properties of ZnO [6-7]. However, they did not give satisfying accurate results for electrical properties. They underestimated the band gap values, misplaced the energy levels for the Zn-3d states and overestimated the crystal-field splitting energy [8]. These functionals ignored the strong hybridization of a localized Zn-3d electron with an O-2p electron. The localized nature Zn-3d electrons at too low binding energies lead to strong hybridization with the O-2p electron, this leads to a reduction of the band gap of ZnO. This hybridization is very important for band gap formation in ZnO, so the band gap of ZnO should rely on the Zn-3d, O-2p orbits [9]. The GGA plus Hubbard parameter (GGA+U) or LDA plus Hubbard parameter (LDA+U) functionals add the orbital-dependent term to the exchange and correlation potential. Therefore, the hybrid DFT–HF functional can be used to obtain agreeable accurate results [10]. Recently, some of the theoretical investigations studied the effects of Hubbard U parameter on p orbitals

(Up) of oxygen and d orbitals (Ud) of transition metals [11]. As a result, the Hubbard parameters are applied on the d orbitals of zinc and p orbitals of oxygen [12].

In addition to studies on wz-ZnO, there are some theoretical studies that relied on density functional theory shed light on the effect of magnesium on the electrical properties of ZnO, in which the LDA and GGA functionals had been used to investigate the electronic properties of wz-MgZnO. The results showed the band gap linearly increased when the mole fraction of magnesium increased but the band gaps' values still have underestimation comparing with the experimental studies [13]. Few of theoretical studies had been used GGA+U to study Mg effects on wz-ZnO properties and the results were very close to the experimental result [14]. Therefore, the GGA+U functional can be used to investigate the electronic and optical properties of wz-MgZnO.

In this work, the electronic and optical properties including the band structures, the density of states, the electron effective masses, the dielectric functions, the refractive indexes, the extinction coefficients and the absorption spectra are calculated for $Mg_xZn_{1-x}O$ in wurtzite phase with different magnesium mole fractions (0%, 6.25%, 12.5%, 18.75%, 25% and 31.25%), respectively using DFT where the GGA+U method is used. On-site Coulomb corrections are applied on the O-2p orbitals (Up) and Zn-3d orbitals (Ud), where the parameters of $U_p = 7$ eV for O and $U_d = 10$ eV for Zn are used. In the calculations, the 2×2×2 super cell is used, the mesh cut-off energy is 500 eV, a mesh of 6×6×5 k-points is used and a broadening of 0.1 eV is applied.

2. ZINC OXIDE

In this chapter, information about the uses of ZnO in industry, crystal structure, band structure, basic electrical properties and basic optical properties will be provided.

2.1 The Uses of Zinc Oxide in Industry

ZnO is an oxidic component naturally obtained as the rare mineral zincide. It is the first industrial zinc compound. Pure ZnO is a white powder and it is used as a major white paint pigment for a long time. The ancient scientists used it to produce the first brass metal; they tried to make precious metal (gold) with it but they failed. By the early 20th century, white, polycrystalline ZnO powder was being used in medical technology. People at that time utilized the ZnO in medical applications such as cosmetics, dental technology, and pharmaceutical manufacturing. Until now ZnO is used to produce face and body cosmetic powder, preparation of sunscreens, bandages, antibiotic lotions, pastes, salves, first-aid tapes, dental cement, etc. In addition, ZnO is used as an additive material to other materials to produce rubbers, plastics, glass, sealants, lubricants, ceramics, batteries, cement, fire retardants, etc. The ZnO has a very high melting point (2248 K), a big cohesive energy (1.89 eV) which leads to high resistance to wear, which makes ZnO the hardest one of the II–VI semiconductors. It has a large adhesion on different substrates, a high resistance to high-temperature electronic degradation, emission spectra on near- UV region, a big piezoelectric coefficient. In addition, ZnO is a transparent semiconductor [15-18].

With the discovery of the extensive properties which were mentioned above, ZnO began to be used in many technological industries. For instance, very high ZnO piezoelectric coefficients that contributed to the development of ZnO-based piezoelectric transducers. In addition, micro-electro-mechanical systems such as sensors, actuators, acoustic devices and electro-optical devices can be produced with ZnO. One of the main properties of ZnO is that the exciton binding energy is greater than the exciton binding energy of GaN. This led to the achievement of the opto- and photo- electronic devices, such as ZnO-based structures to produce near-UV emission optoelectronic devices and MgZnO/ZnO based heterostructures to provide the deep-UV emission optoelectronic devices.

ZnO has been widely used to produce catalysts, photonic materials, small size devices such as windows materials for produce the flat panel displays, transparent electrodes and transparent conduction in a solar cell, flat panel displays, gas sensors and transparent conduction films. In addition, ZnO is also used to produce surface acoustic wave resonators, bulk and thin film acoustic wave resonators. ZnO is used to manufacture UV-diode emitters, transistors, ZnO- based transducers, detectors, optically transparent electrically conducting films, optically pumped laser, Metal Semiconductor Metal (MSM)-type UV detectors, surface acoustic wave devices, UV excitonic lasers, tunable UV photo-detectors, light emitting diodes (LEDs), laser diodes, deep ultra-violet light emitters, piezoelectric transducers and varistors [19].

2.2. Crystal Structure

Bulk ZnO can be obtained in three types of crystal structures. The most thermodynamically stable phase under ambient conditions is wurtzite ZnO (wz-ZnO) where crystallizes in a hexagonal lattice, with a belonging to space group $P_{63}mc$. Most of the investigation focuses on wz-ZnO to study its optical and electronic properties. ZnO can be obtained in a zinc blende phase (zb-ZnO) but it can be grown stable on a cubic substrate and specific growth conditions, it belongs to space group F-43m. And, the rock-salt phase (rs-ZnO) can be obtained at a relatively high pressure between 8-10 GPa. It belongs to space group Fm-3m [20]. Figure 2.1 shows the unit cell structures for the three phases of ZnO where the big gray and red balls denote Zn and O atoms, respectively. In cubic zinc blende (zb) or hexagonal wurtzite (wz) zinc oxide structures, the primitive cell contains two Zinc atoms and two Oxygen atoms. The primitive cell formed by a tetrahedron, where the zinc atom is located at the centers and four oxygen atoms are located at the corners and vice versa. This tetrahedral space orientation is due to strong sp^3 covalent bonding nature. In addition to covalent nature, ZnO has an ionic nature that makes the energy gap increases more than what is expected to be obtained from covalent bonding. Therefore, ZnO takes a place between covalent and ionic semiconductors [8]. The ionicity impact sets more electrons on oxygen atoms giving the charge density more s and p characteristics of these elements in the valence band, this leads to gaps at the edge of the Brillouin region compared with totally covalent bonding materials. That means, there are flatter bands in the Brillouin region.
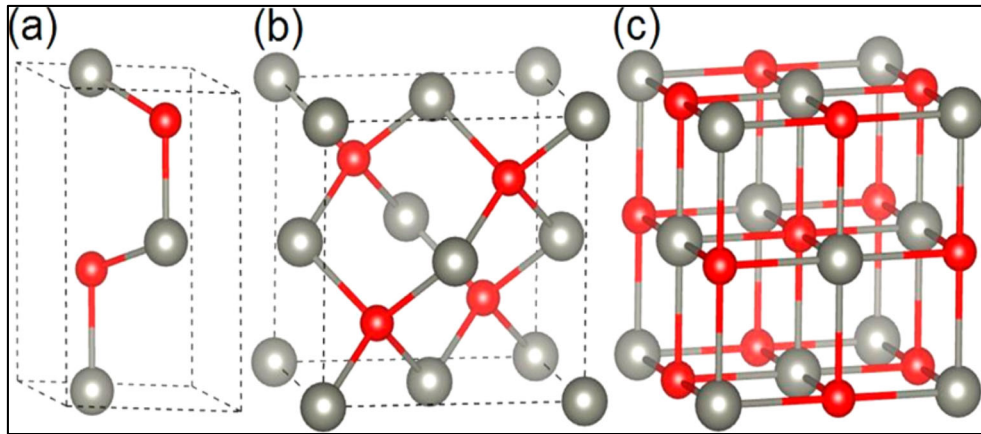
Figure 2.1. Unit cell structures of zinc oxide, (a) wz-ZnO, (b) zb-ZnO, and (c) rs-ZnO [12]

The difference between the zb-ZnO and wz-ZnO is that the zb-ZnO is cubic whereas the wz-ZnO is a distortion of the cube in the [111] direction occurring in the z direction in the wurtzite [21] as shown in the figure 2.2
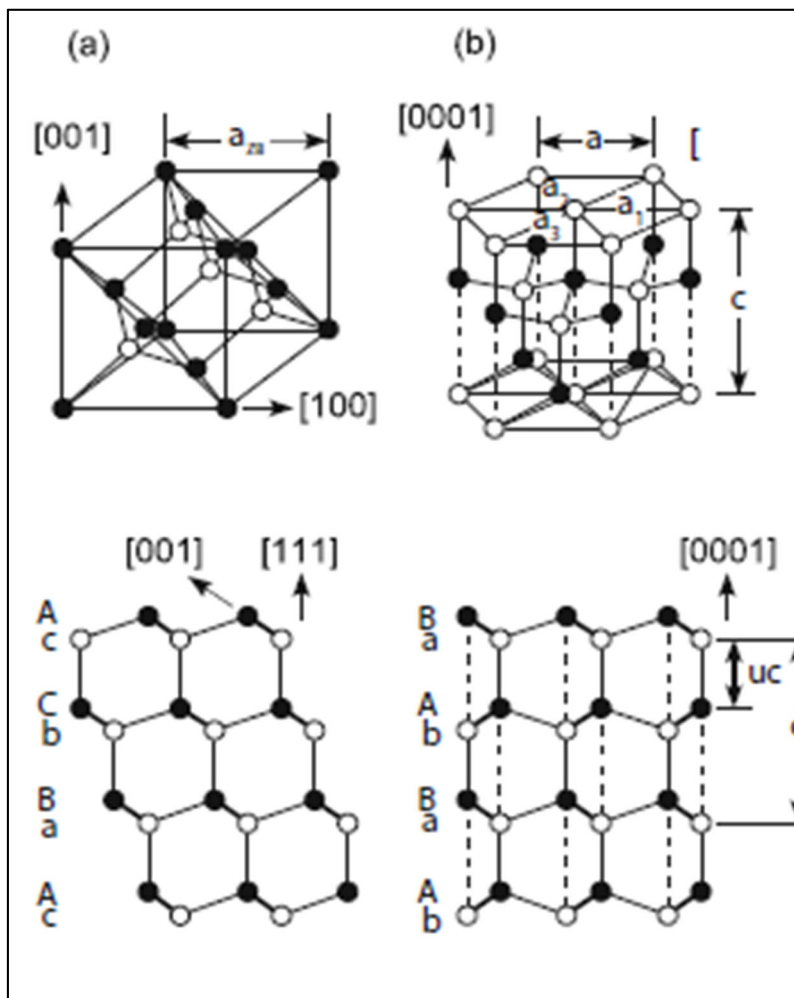
Figure 2.2. The difference between (a) zb-ZnO and (b)wz-ZnO [21]

The unit cell is hexagonal with two different lattice parameters c and a, where c lattice parameter is the axial lattice parameter (unit cell height) and a lattice parameter is the basal plane lattice parameter (the edge length of the basal plane hexagon). The c lattice parameter is perpendicular to the basal plane. There are two bond angles α and β. The internal parameter u is the length of the bond parallel to the c-axis divided by the c lattice parameter, $u=b/c$; where b is the length of the bond parallel to the c-axis. In figure 2.3, the structure consists of two interpenetrating hexagonal close packed (hcp) sub-lattices. In each sub-lattice, there is one kind of atom displaced with respect to other along the threefold c-axis by the amount of the internal parameter. Each sub-lattice having 4 atoms per unit cell, where each atom of the same kind is enclosed by atoms of the other kind, or vice versa, that are arranged at the tetrahedron's edges.
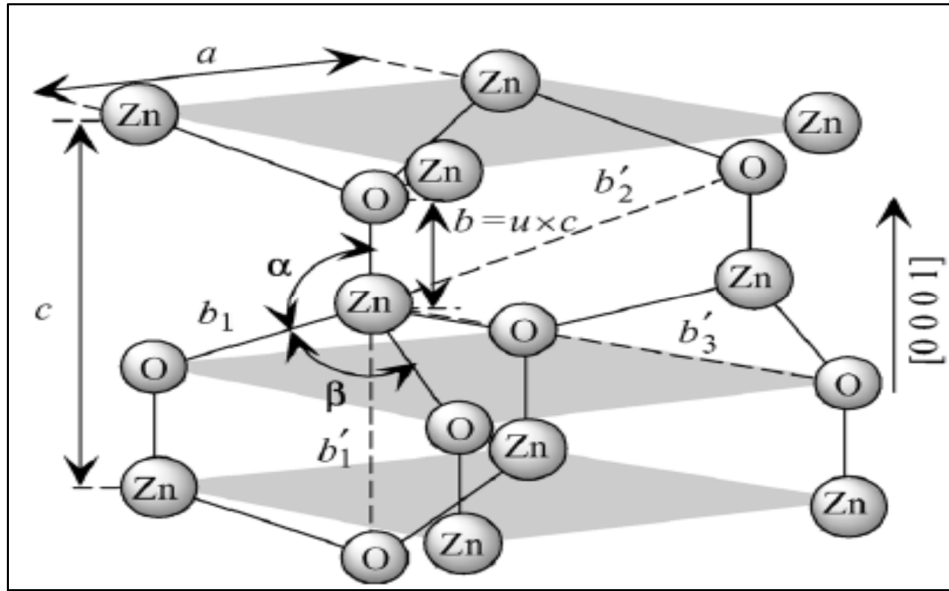
Figure 2.3. Illustration of wz-ZnO structure [22]

The u parameter can be defined as:

$$u = \frac{1}{3} \left(\frac{a}{c}\right)^2 + \frac{1}{4} \tag{2.1}$$

The bond angles can be defined as:

$$\alpha = \frac{\pi}{2} + \cos^{-1}\left[\left(\frac{1}{\sqrt{1 + 3\left(\frac{c}{a}\right)^2 \left(\frac{1}{2} - u\right)^2}}\right)\right] \tag{2.2}$$

$$\beta = 2 \sin^{-1} \left[\left(\frac{1}{\sqrt{\frac{4}{3} + 4 \left(\frac{c}{a}\right)^2 \left(\frac{1}{2} - u\right)^2}} \right) \right] \qquad (2.3)$$

There are two kinds of nearest-neighbor bond lengths, b is the bond length to nearest-neighbor along the c-direction, b_1 is the bond length off c-axis to nearest-neighbor, they can be defined as:

$$b = cu \qquad (2.4)$$

$$b_1 = \sqrt{\frac{1}{3} a^2 + \left(\frac{1}{2} - u\right)^2 c^2} \qquad (2.5)$$

There are 3 different second-nearest neighbors, they specified as b_1', b_2' and b_3', where b_1' is second-nearest neighbor along the c-direction, there are six of b_2' and three of b_3', they can be defined as:

$$b_1' = c(1 - u) \qquad (2.6)$$

$$b_2' = \sqrt{a^2 + (cu)^2} \qquad (2.7)$$

$$b_3' = \sqrt{\frac{4}{3} a^2 + \left(\frac{1}{2} - u\right)^2 c^2} \qquad (2.8)$$

There is a strong relation between the ratio of the lattice parameters and u parameter, when one of them increases, the other decreases so that the four tetrahedral bond lengths are almost constant if a small difference of tetrahedral angles happened because of the long-range polar interactions [22].

The most significant surfaces are the (0001) and $(000\bar{1})$ which are defined as a basal plane, $(10\bar{1}0$) and $(11\bar{2}0)$ which are defined as a prism plane and $(11\bar{2}1)$ which is defined as a pyramidal plane. The (0001) plane is set by Zn atoms only, while the $(000\bar{1})$ surface is set by oxygen atoms only, as shown in the figure 2.4.
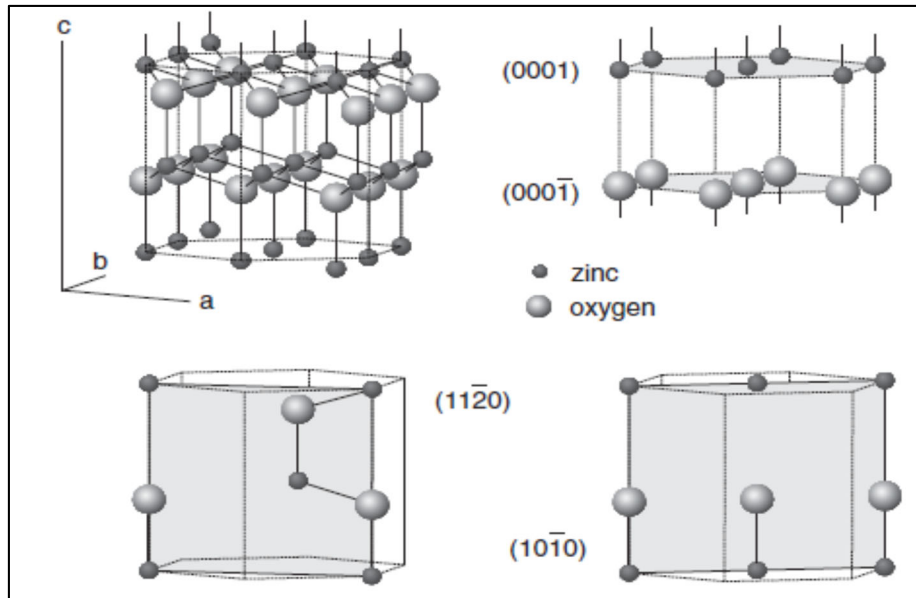
Figure 2.4. The basic surfaces of ZnO [22]

There are differences in these values between the ideal wurtzite structure and real wurtzite structure. In the ideal wurtzite structure, the ratio between the lattice parameters is equal $c/a = \sqrt{8/3} = 1.633$ and the value of the internal parameter is $u = 3/8 = 0.375$, the bond angles are (α and β) equal to 109.47°. The lattice parameters change according to the surrounding conditions, where they can be influenced by temperature, composition, stress, impurities and free charge. In addition, the c/a ratio related with the electronegativity difference between two types, where the components with small differences exhibit small divergence from the ideal c/a ratio, and vice versa. Therefore, in the real lattice, the lattice parameters ratio c/a and u parameter deviate from their values in the ideal lattice because of the lattice stability, ionicity, point defects and extended defects. For ZnO, it was observed that the ratio between the lattice parameters (c/a) that obtained experimentally is less than its value in the ideal lattice, as is the case of GaN [22-23].

2.3. Band Structure

In individual atoms, electrons revolve around the nucleus in specific orbitals, of crystals which consist of a lot of atoms these orbitals of single atoms interfere to form energy bands. There are two permitted bands the valence (VB) and the conduction band (CB). The valence band which is defined as the highest occupied energy band where at 0K whereas a conduction band is defined as the lowest range which has vacant electronic states at 0K.

In terms of conductivity, semiconductors are materials that are located between conductors and insulators. At the low temperature, the semiconductor behaves like an insulator whereas at the room temperature the semiconductor behaves like a conductor.

In the metals, there is an overlap between the VB and CB that makes the current conduction so easy. Whereas, in both semiconductors and insulators; there is an energy gap between the lowest unoccupied state of the CB and the highest occupied energy state of the VB, in which electrons are forbidden from occupying. This difference is defined as the forbidden band. In the insulators, the VB is completely full, and the CB is completely empty. In addition, the band gap is relatively large (E_g >> 4 kT) so that the valence electrons can't move to the CB and can't contribute to the conductivity, even so at temperatures that are near to the room temperature.

 It is clear from the figure 2.5 that the forbidden gap in the most semiconductors is smaller than insulators which explains why semiconductors have electrical conductivity at temperatures that are near to the room temperature.
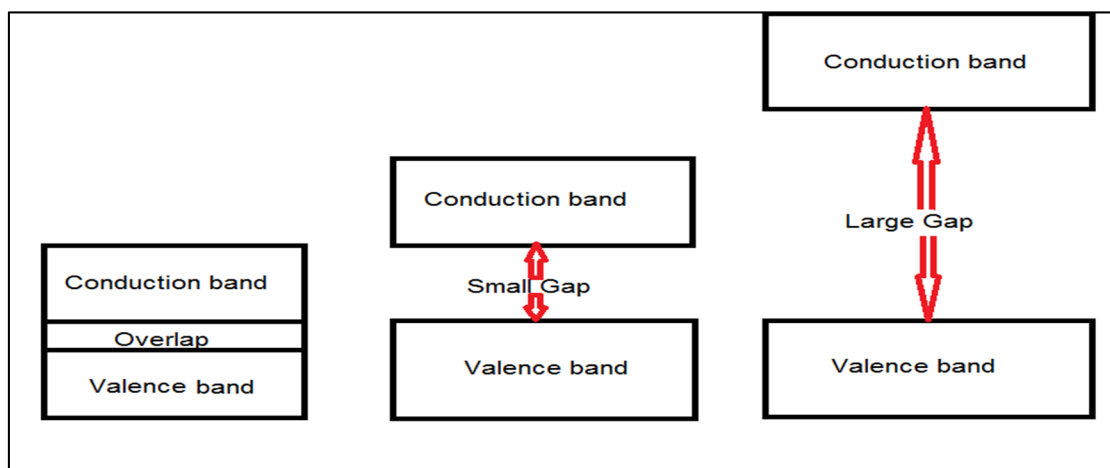
Figure 2.5. Representation of the band structures of a conductor, a semiconductor and an insulator, respectively

Electronic band structure graphs are defined as curves of energy as a function to wave vector (k -vector) for a number of bands which are sampled in reciprocal space. In the reciprocal lattice crystal, if lattice vectors were drawn from the origin point to the nearest neighboring points (in the three dimensions) and planes vertically bisecting these vectors

were drawn, the area surrounding the original point will be obtained, which is the smallest polyhedron bounded by planes vertically bisecting the reciprocal lattice vectors, which is defined as the first Brillouin zone, also is defined as the primitive cell in reciprocal lattice. For wurtzite structures, the most important symmetry points are A which is defined as the center of a hexagonal face, L which is defined as the middle of an edge joining a rectangular and a hexagonal face, M which is defined as the center of a rectangular face, K which is defined as the middle of an edge joining two rectangular faces, H which is defined as the corner point and Γ which is defined as the center of the Brillouin zone [24], as shown in the figure 2.6.
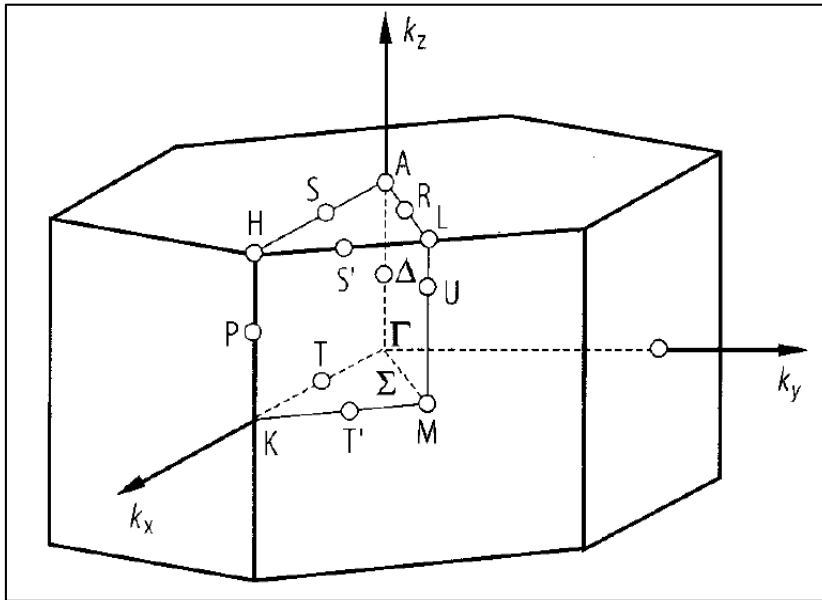
Figure 2.6. The first Brillouin zone for hexagonal structure and the symmetry points [24]

ZnO is one of the best-known semiconductors with tetrahedral bonds, in which the cation and anion s- and p-orbitals compose sp^3-hybrids, which overlap to obtain bonding and anti-bonding combinations. The valence band is primarily obtained from the covalent bonding orbitals (p and s), while the conduction band is derived from anti-bonding orbitals [24].

ZnO has a direct band gap semiconductor since the conduction band minimum (CBM) and the valence band maximum (VBM) are located at Γ point, as shown in the figure 2.7.
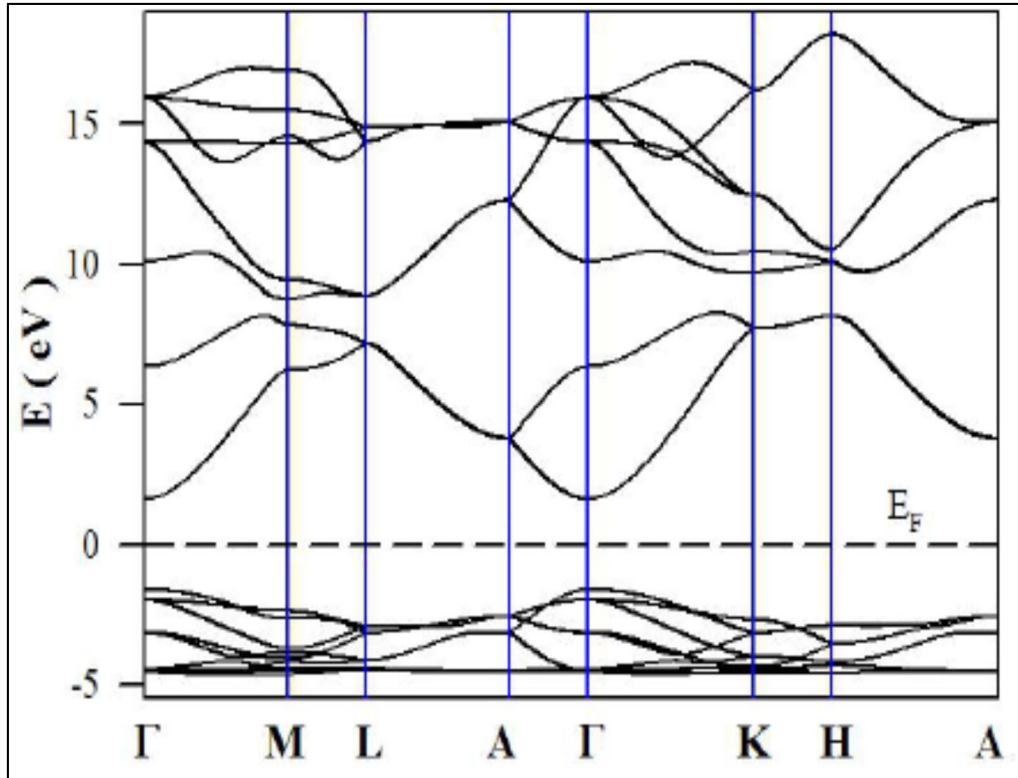
Figure 2.7. Band gap of pure wz-ZnO

The wz-ZnO structure doesn't have inversion symmetry along the c-axis. In addition, the ratio *c/a* deviates from the ratio of an ideal structure and the ionic nature of the bonds, these reasons create crystal polarity between the two opposite faces along the c-axis. There are non-polar and polar surfaces in ZnO. The polar one is either negatively or charged positively. The positively charged surfaces are totally ended with zinc cations (Zn^{2+}), while the negatively charged surfaces are entirely ended with oxygen anions (O^{2-}) [26].

The O^{-} (000$\bar{1}$) and Zn^{-} (0001) surfaces are the extreme known polar surfaces with dipole moment along the c-axis, as shown in the figure 7. An electrical potential occurs between these Zn^{-} (0001) and O^{-} (000$\bar{1}$) surfaces which create a strong piezoelectric effect. Polarity difference between the surfaces may impact the experimental results on the two surface terminations, for example, barrier height formation of a Schottky contact. The most common nonpolar surface is (10$\bar{1}$0) surface (m-plane), this surface is obtained with the same number of Oxygen and Zinc atoms. In the polar surfaces, the charges in these surfaces are fixed and non-transferable. The ZnO structure has an arrangement that decreases the electrostatic energy. Despite the large electrostatic reactions, the ZnO polar

surfaces don't suffer from surface reconstruction. In addition, ZnO polar surfaces are stable [27-28] as shown in the figure 2.8.
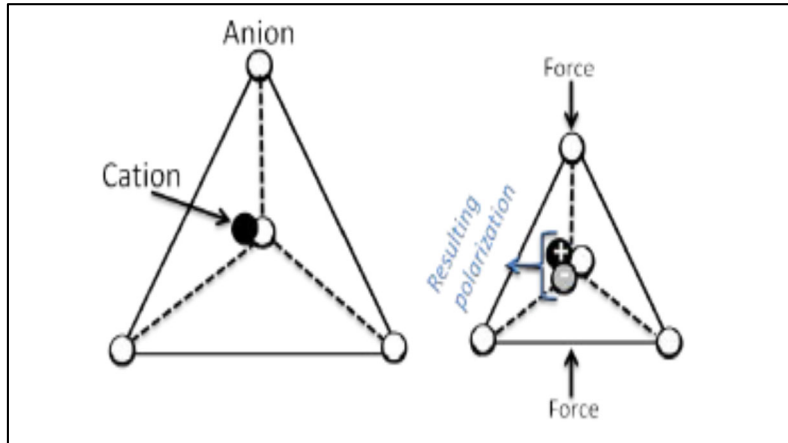
Figure 2.8. Diagram for tetrahedron coordination of ZnO and the produced polarization

2.4. Basic Electrical Properties

ZnO is one of the transparent conducting oxide semiconductors (TCOs). In addition, the existence of active native defects and impurities with donor ionization energies which ranging from 10 to 100 meV at concentrations ranging from 10^{15} to 10^{17} cm^{-3}. ZnO shows defect dominated n-type conductivity at room temperature. ZnO has a wide band gap (3.37 eV at 300K), which is the reason of defect- or impurity-dominated conductivity, that means ZnO is transparent and native n-type conductive concurrently. It was unable to obtain to primary electronic properties of intrinsic ZnO due to difficulty in obtaining enough O incorporation into the samples, therefore the difficulty in the achievability of sufficiently high-quality materials. Therefore, most experimental investigations that studied the electronic properties of pure ZnO mostly used n-type doped ZnO samples [29].

The native (intrinsic) defects are deficiencies due to a change in the position of the fundamental elements in the lattice crystal, including vacancies, interstitials, and anti-sites, as shown in figure 2.9. The vacancy is the absent atom at regular lattice sites. The interstitial is the additional atom occupying interstice inside the lattice which is constituent atom of the lattice crystal. Anti-site is an oxygen atom occupying a zinc atom lattice site or vice versa.
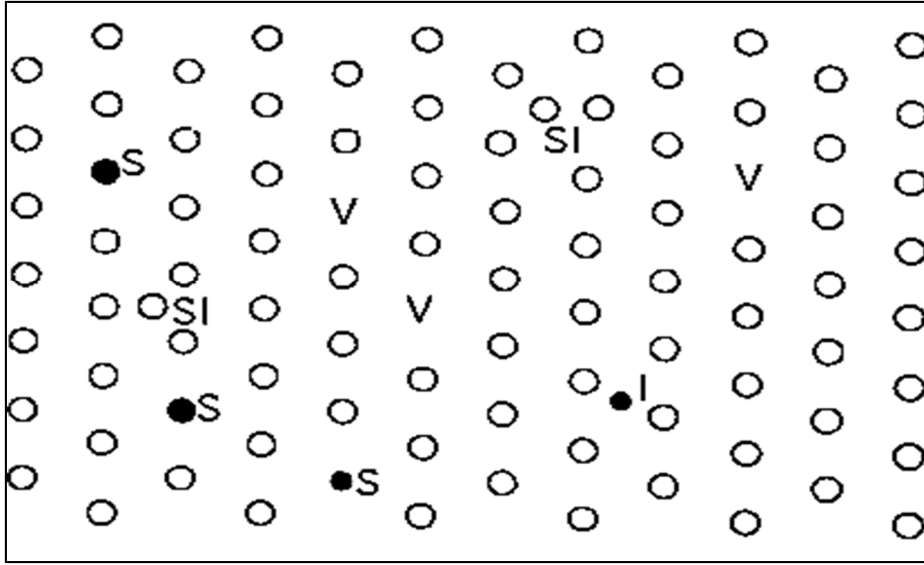
Figure 2.9. The native (intrinsic) defects, where V refers to the vacancies, I refers to the inter-stitials, S refers to anti-sites and SI self-interstitials

The native defects according to behavior are classified into donor-like native defects and acceptor-like native defects. In ZnO, the donor-like native defects are zinc interstitials, oxygen vacancies, and zinc anti-sites which behave as deep donors as well as shallow donors with high formation energies. The acceptor-like native defects are oxygen interstitials at octahedral sites, zinc vacancies and oxygen interstitials which behave as deep acceptors. The oxygen interstitials are stable as electrically inactive at split interstitials sites, but they are electrically active at the octahedral sites. Zinc vacancies are the reason for the green luminescence [30].

In ZnO, the native n-type conductivity is assumed because of electrically active native point defects like Zn interstitials and O vacancies. In addition, unintentional impurities contribute to the native n-type doping such as hydrogen that exists in high concentration within ZnO crystals in all growth methods and diffuse easily through ZnO with activation energy about 39 meV [31]. The n-type ZnO can be obtained by doping with group III elements such as In, Ga and Al where Zn is replaced with group III elements, or by doping with group-VII elements like Cl and I where O is replaced with group-VII elements. The n-type doped ZnO can be easily obtained but controlling n-type doping concentration is still difficult, which change according to growth processes. Al-/or Ga- doped ZnO can be obtained with carrier concentrations more than 10^{21} cm^{-3} and resistivity lower than 10^{-4} Ω.cm[32]. Obtaining p-type doped ZnO is still very hard, achieving that remained a

challenge. The reasons for the difficulty of achieving the p-type doping are due to the following:

1) A few candidates have appropriate properties to be a shallow acceptor in ZnO crystal structure, 2) the dopants mostly have a low solubility in ZnO which produce low carrier concentrations, 3) Hydrogen incorporation and the effects of self-compensating from native defects (oxygen vacancy and Zinc interstitial) [31].

Alkali metals (Li, K and Na) and group-V elements (N, As and P) are the major p-type candidates, Zinc is replaced with alkali metals while oxygen is replaced with group-V elements. Also, the p-type ZnO can be happened by co-doping of III-V groups, like Al-N [32].

2.5. Basic optical properties

In terms of optical properties, ZnO have special features that can be used in applications, the huge exciton binding energy (60 meV) which increase the UV lasers efficiencies, the changeable band gap from 2.8 eV to 4 eV, the low threshold for optical pumping lasers at 0K and the ferromagnetic properties with a Curie temperature above 300 K for ZnO can be discovered by alloying ZnO with Mn or one of the transition metals [33].

The optical properties are affected by the intrinsic and extrinsic defects. The extrinsic defects include the defects and the impurities which originated discrete states in the band gap. The intrinsic defects include excitonic effects that also have two types, the free exciton (include the excited states and their transition) and the bound exciton. A lower crystal quality can be obtained because of the scattering or alloying, which makes the phonon-mode broadening parameter bigger. Thus, information about the quality of crystal can be known by studying the phonon-mode frequency and the phonon-mode broadening parameter [34].

In photoluminescence spectra of ZnO shows three regions of emission. Near-ultraviolet emission region (375 nm) due to the exciton nature, which includes the free exciton emission, bi-exciton emission, and bound exciton emission. Green emission region that extent (510 nm) due to lattice native defects such as Zn vacancies. Yellow-orange region (590 nm) [35]. The presence of the native effects can affect the absorption spectra which

change the actual band gap and shift the light absorption, such as O vacancies which shift the optical absorption band from the ultraviolet area to the red or orange area [14].

The important optical functions can be obtained from the dielectric function $\varepsilon(\omega)$ like refractive index function $n(\omega)$, the extinction coefficient function $k(\omega)$, and the absorption coefficient function $\alpha(\omega)$.

The complex dielectric response function in linear response area, which can be defined as:

$$\varepsilon(\omega) = \varepsilon_1(\omega) + \varepsilon_2(\omega) \tag{2.9}$$

where the $\varepsilon_2(\omega)$ is the imaginary part of the dielectric function and the $\varepsilon_1(\omega)$ is the real part of the dielectric function. The real part $\varepsilon_1(\omega)$ and the imaginary part $\varepsilon_2(\omega)$ of the dielectric function can be obtained from the dispersion relation of Kramers–Kronig.

The extinction coefficient and the refractive index can be defined as

$$n = \sqrt{\frac{\sqrt{\varepsilon_1{}^2 + \varepsilon_2{}^2} + \varepsilon_1}{2}} \tag{2.10}$$

$$k = \sqrt{\frac{\sqrt{\varepsilon_1{}^2 + \varepsilon_2{}^2} - \varepsilon_1}{2}} \tag{2.11}$$

The extinction coefficient and refractive index are determined by the complex dielectric constant, while the optical absorption coefficient is obtained by the extinction coefficient through the equations below

$$\alpha = \frac{2\,\omega\,k}{c} = \frac{4\,\pi\,k}{\lambda} \tag{2.12}$$

$$n + k = \sqrt{\varepsilon_r} \tag{2.13}$$

Where the ε_r is the complex dielectric constant, α the optical absorption coefficient, k the extinction coefficient and λ is the wavelength [36].

The refractive index is determined by the real part of the dielectric function. Thus, both have the same dependence on energy (wavelength). Whereas, the extinction coefficient and

the absorption coefficient are obtained by the imaginary part of the dielectric function. Thus, all of them have the same dependence on energy (wavelength).

Table 2.1. Some properties of ZnO, MgO, and GaN [37-39]

property	ZnO	MgO	GaN
Phase type	wurtzite	rock-salt	wurtzite
Band gap energy (eV)	3.37	7.8	3.4
Space group	P63mc	F3m3	P63mc
a parameter (Å)	3.25	4.25	3.189
c parameter (Å)	5.206	—	5.185
c/a	1.601	—	1.626
Internal parameter u	0.382	—	0.376
Density (g.cm^{-3})	5.61	3.58	6.51
Intrinsic carrier concentration (cm^{-3})	$< 10^6$	n/a	n/a
Phonon frequency gap (THz)	3.98	n/a	6.11
excitation binding energy (meV)	60	80	18-28
Electron effective mass (m_e)	0.24	0.38	0.2
Hole effective mass (m_e)	0.5 – 0,59	n/a	0.8
Static dielectric constant $\varepsilon\,(0)$	8.66	9.83	9.5
High frequency dielectric constant $\varepsilon\,(\infty)$	3.75	2.95	5.15
Refractive index	2.008-2.029	1.735	2.308-2.380
Bulk modulus (GPa)	183(7)	160.3(3)	195

3. MAGNESIUM ZINC OXIDE

In this section, information about the crystal structure, band structure, basic electrical properties and basic optical properties of $Mg_xZn_{1-x}O$ will be provided. In addition, the information about MgZnO/ZnO heterostructures will be provided.

3.1. Crystal Structure

$Mg_xZn_{1-x}O$ is a ternary compound can be obtained by alloying wz-ZnO by rs-MgO. The ZnO has a hexagonal lattice with two lattice parameters a=3.25 Å and b = 5.20 Å, whereas the MgO has a cubic structure with the lattice parameter a = 4.25 Å. So, the $Mg_xZn_{1-x}O$ has two types of crystal lattices wurtzite magnesium zinc oxide (wz-$Mg_xZn_{1-x}O$) and rock-salt magnesium zinc oxide (rs-MgZnO). The crystal structure type determined by the Mg (or Zn) mole fraction. wz- $Mg_xZn_{1-x}O$ can be obtained until the 37% Mg mole fraction, while rs- $Mg_xZn_{1-x}O$ can be obtained when the Mg mole fraction bigger than 62%. There is a mixed phase which can be obtained when the Mg mole fraction between the 37% and 63% [40], as can be seen from the figure 3.1.
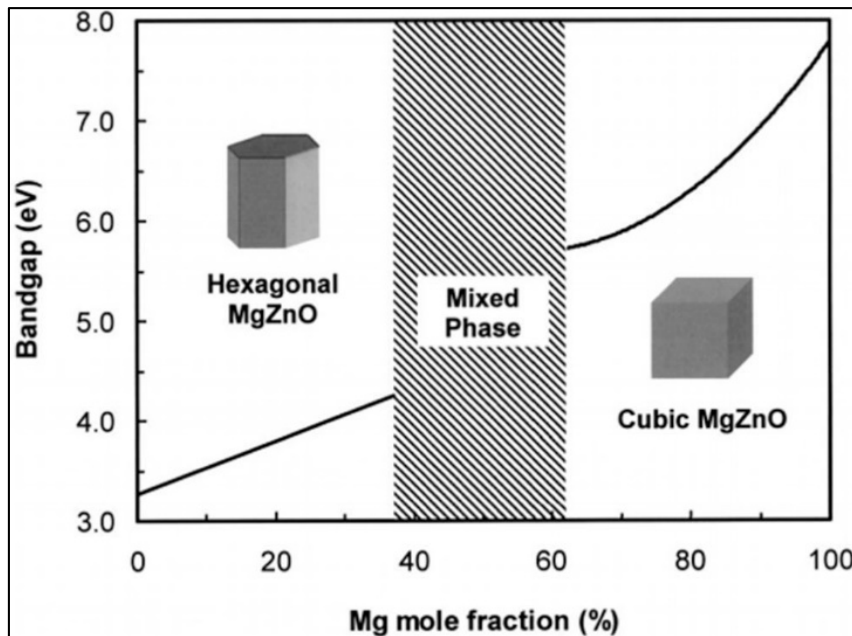

Figure 3.1. The band gap energy of MgZnO, where the changing of crystal structure for $Mg_xZn_{1-x}O$ is illustrated [40]

3.2. Basic Electrical Properties

The electrical properties of $Mg_xZn_{1-x}O$ changes when the $Mg_xZn_{1-x}O$ crystal structure type changes, that means the electrical properties of $Mg_xZn_{1-x}O$ is determined by the Mg mole fraction. The band gap energy changes with the concentration of magnesium within the crystal structure. Also, the lattice parameters, bond length, the internal parameter, the ratio between the lattice parameters, the electron effective mass and hole effective masses change according to the concentration of magnesium within the crystal structure.

The lattice parameters can be calculated using this formula,

$$\begin{bmatrix} a \\ b \\ c \end{bmatrix} = \begin{bmatrix} \varepsilon_{xx} & \varepsilon_{xy} & \varepsilon_{xz} \\ \varepsilon_{yx} & \varepsilon_{yy} & \varepsilon_{yz} \\ \varepsilon_{xz} & \varepsilon_{zy} & \varepsilon_{zz} \end{bmatrix} \begin{bmatrix} a_0 \\ b_0 \\ c_0 \end{bmatrix} + \begin{bmatrix} a_0 \\ b_0 \\ c_0 \end{bmatrix} \tag{3.1}$$

$$\varepsilon_{xx} = \varepsilon_{yy} = \frac{a - a_0}{a} \tag{3.2}$$

$$\varepsilon_{zz} = -2 \left(\frac{c_{13}}{c_{33}} \right) \varepsilon_{xx} \tag{3.3}$$

where a_0, b_0, and c_0 are the lattice parameter of wz-ZnO, the tensor is the strain tensor, c_{ij} is stiffness constant and a, b, and c are the lattice parameter of wz-$Mg_xZn_{1-x}O$. The strain tensor is obtained by the Hooke's law and Vegard's rule [41].

Some of the experimental and theoretical studies calculated the lattice parameters of wz-$Mg_xZn_{1-x}O$ [41-42, 13] as can be seen from the table 3.1.

Table 3.1. The lattice parameters of wz- $Mg_xZn_{1-x}O$ [41-42, 13]

Lattice Parameter	Theoretical [41]	Experimental [42]	Theoretical [13]
a (Å)	$3.250 + 0.036\,x$	$3.2491 + 0.047\,x$	$3.28162 + 0.06653\,x$
c (Å)		$5.2042 - 0.072\,x$	$5.31564 - 0.15373\,x$

The figure 12 shows the lattice parameters of wz-$Mg_xZn_{1-x}O$ as a function to the Mg mole fraction. The lattice parameter a rises as the Mg mole fraction rises, whereas the lattice parameter c decreases when the Mg mole fraction increases [14].

As mentioned previously, the band gap energy changes when the Mg mole fraction changes. Some of the theoretical and the experimental studies investigated the band gap energy of wz-Mg$_x$Zn$_{1-x}$O which increases linearly as Mg mole fraction increases. Christian Franz *et al*. calculated the band gap energy of wz-Mg$_x$Zn$_{1-x}$O up to 30% Mg mole fraction, the results show a linear dependence on Mg mole fraction which founded as follows $E_g = 1.08 + 2.03\,x$ [43].
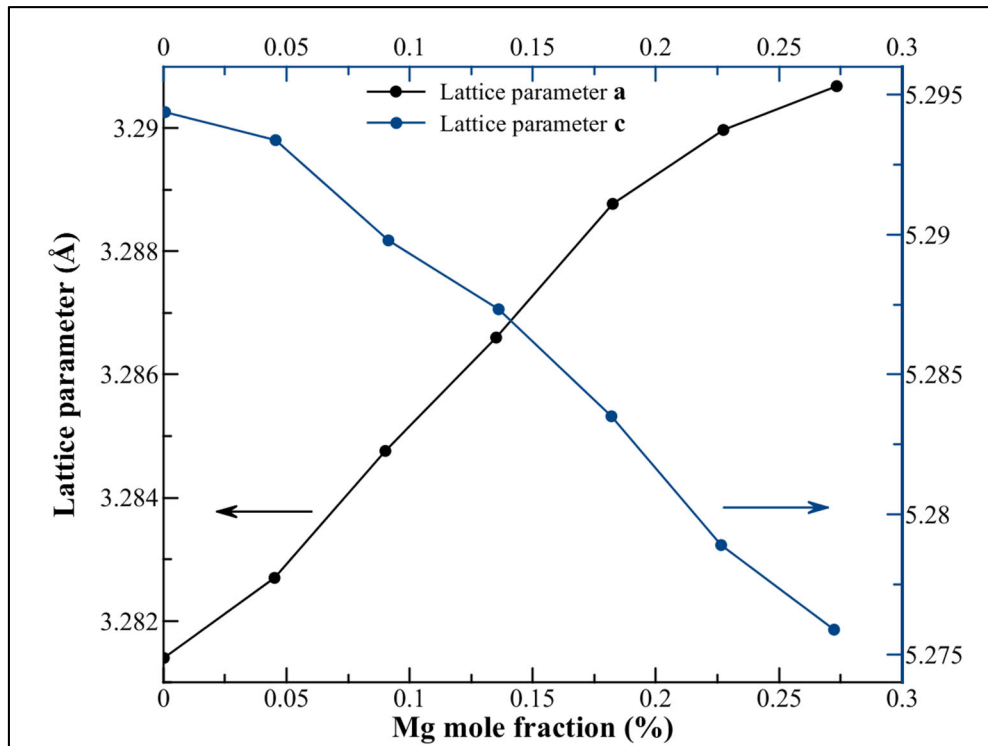
Figure 3.2. The Mg mole fraction dependent lattice parameters of wz-Mg$_x$Zn$_{1-x}$O

While the results of Ohtomo *et al*. show a linear dependence on Mg mole fraction which appeared as follows $E_g = 3.3 + 2.1\,x$ up to 33% Mg mole fraction [44]. Likewise, Chen *et al*. results obtained $E_g = 3.32 + 2\,x$ for Mg mole fraction lower than 33% [45]. Wu *et al*. results show this equation $E_g = 3.384 + 1.705\,x$ for Mg mole fraction between 0 and 44% [46]. The figure 3.3 shows the results of Christian Franz *et al*. where the band gap increases linearly, as mentioned above. Few theoretical studies showed that the band gap energy has a nonlinear dependence on Mg mole fraction [47] between 0 and 100% Mg mole fraction which can be written as

$$E_g^{(\Gamma-\Gamma)}(x) = 2.754 + 0.104\,x + 1.861\,x^2$$

$E_g^{(M-\Gamma)}(x) = 1.376 - 1.379\,x + 4.981\,x^2$, as shown in figure 3.4.

Some of the theoretical studies showed a linear correlation between the electron effective mass and Mg mole fraction [43] whereas other studies suggested a quadratic dependence [48]. Figure 3.5 shows the electron effective mass as a function to Mg mole fraction where there is a linear dependence that is written as $\dfrac{m^*}{m_e} = 0.186 + 0.267\,x$. Whereas the hole effective mass change randomly as the Mg mole fraction increase [43].

Figure 3.3. The band gap energy of wz-$Mg_xZn_{1-x}O$ as a function to Mg mole fraction

Figure 3.4. The direct and indirect band gap energy of wz-$Mg_xZn_{1-x}O$. as a function to Mg mole fraction

Figure 3.5. The Mg mole fraction dependent electron effective mass of wz-$Mg_xZn_{1-x}O$

For the wz-$Mg_xZn_{1-x}O$, the valence band is formed mostly from the hybridization between the Zn-3d state and the O-2p state, as the case of wz-ZnO. Whereas the conduction band is obtained from the hybridization between the Zn-4s state and the Mg-3s st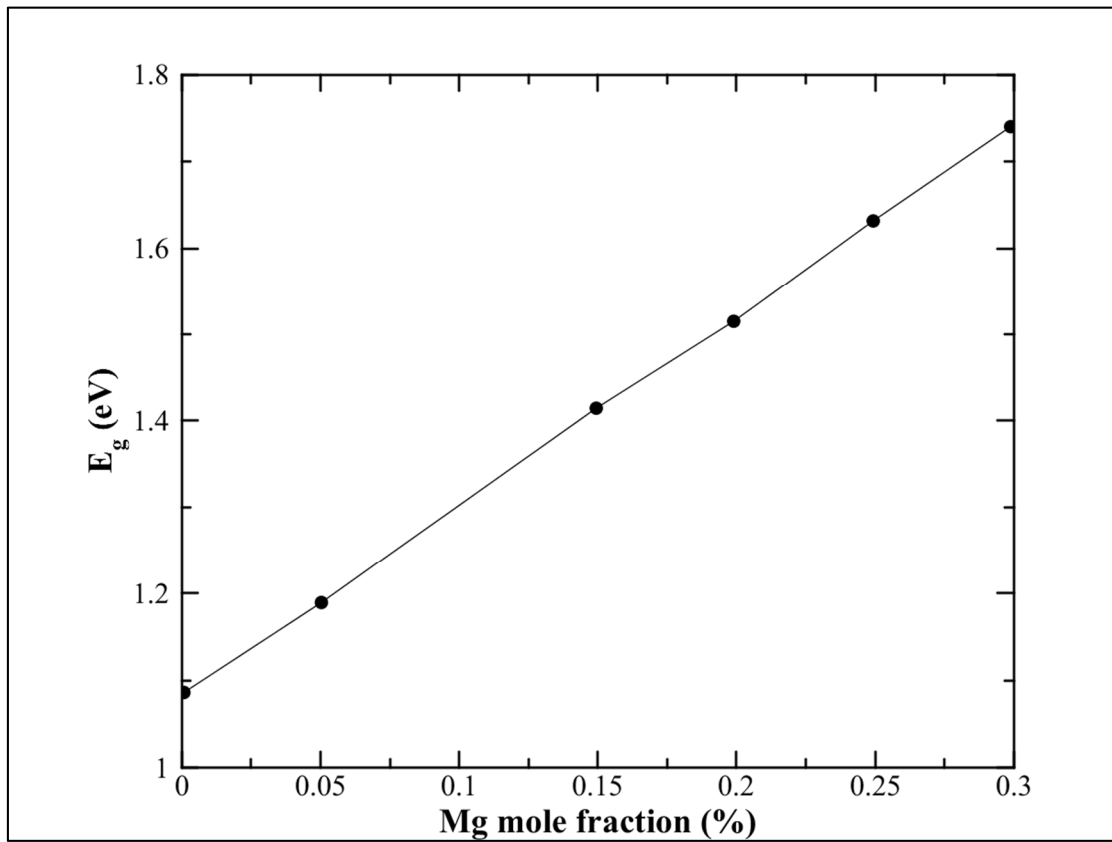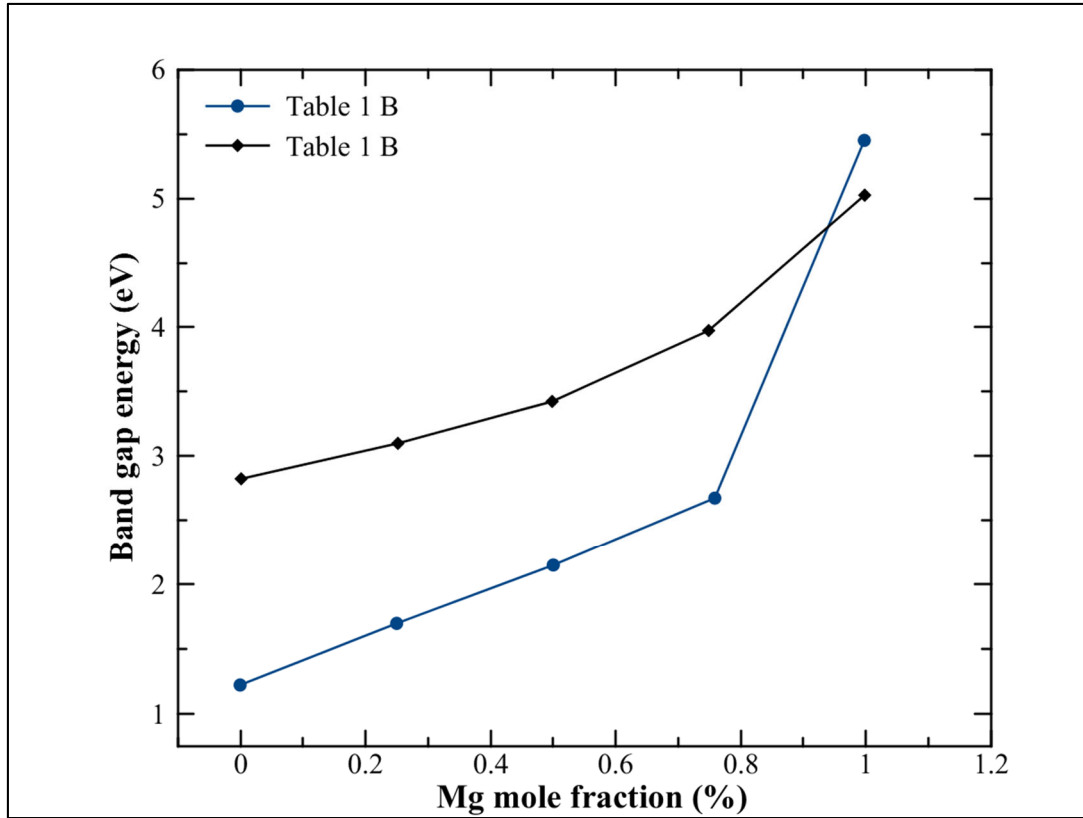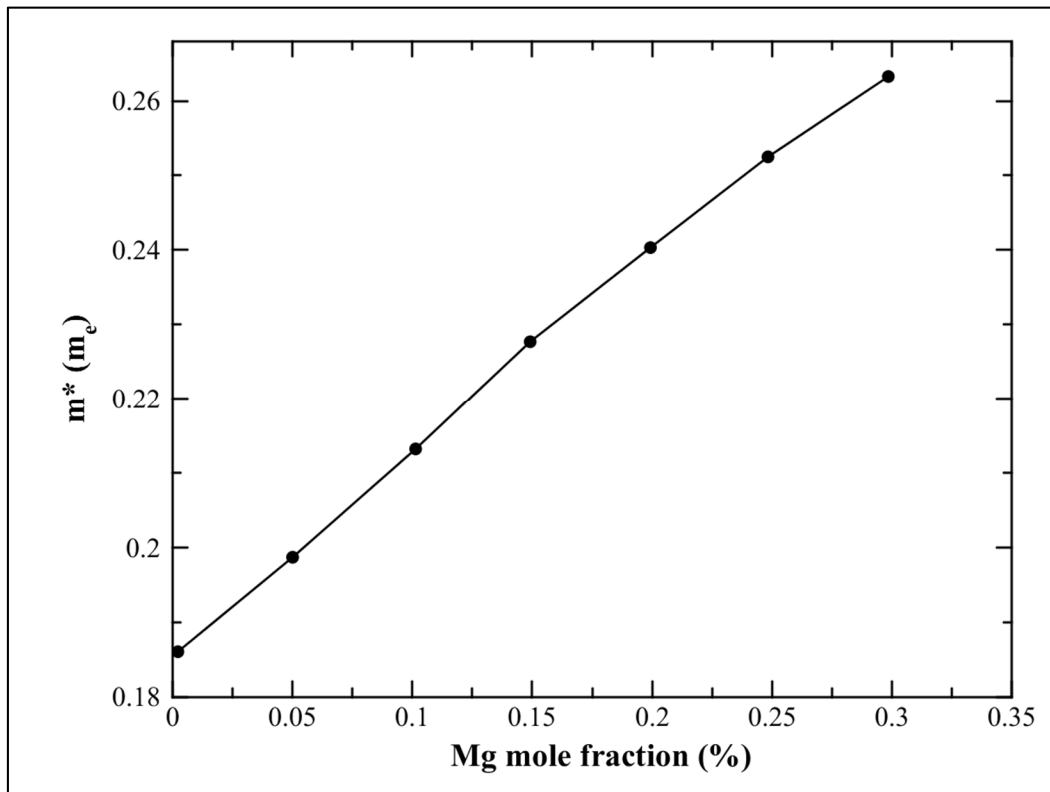ate which effect on the CBM that can move it toward the higher energies range. This explains why the band gap energy for wz-$Mg_xZn_{1-x}O$ bigger than for the wz-ZnO [13].

The $Mg_xZn_{1-x}O$ shows native n-type conductivity at room temperature because of the donor-like native defects such as zinc interstitial and oxygen vacancies, as the case of wz-ZnO. The n-type $Mg_xZn_{1-x}O$ can be obtained easier than the p-type $Mg_xZn_{1-x}O$ which is obtained difficulty, as the case of ZnO. Theoretically, the p-type $Mg_xZn_{1-x}O$ can be obtained by doping with alkali metals (Li, Na and K) and group-V elements (N, P and As) whereas the n-type $Mg_xZn_{1-x}O$ can be obtained by doping with Al, Ga and Si, as the case of ZnO. B. Yao *et al*. found that N doped $Mg_xZn_{1-x}O$ film which was grown using plasma-assisted molecular beam epitaxy method behaved as n-type doped $Mg_xZn_{1-x}O$. Whereas after annealing it for 1 hour at 600 °C in an O_2 flow, behaved as p-type doped $Mg_xZn_{1-x}O$ with a hole concentration about 6.1×10^{17} cm^{-3} and a mobility of about 6.42 $cm^2/V.s$ [49].

3.3. Basic Optical Properties

The $Mg_xZn_{1-x}O$ is a transparent conducting oxide semiconductor. Mg^{+2} (0.57Å) and Zn^{+2} (0.60Å) have so close ionic radius, that make the lattice without much distortion. The $Mg_xZn_{1-x}O$ has a wide changeable band gap energy (3.37-7.8) eV according on the Mg content within the crystal structure. The $Mg_xZn_{1-x}O$ can be grown at low temperature (75-100 C°). The MgO has bond strength stronger than ZnO that makes the $Mg_xZn_{1-x}O$ more stability than the ZnO. In addition, MgZnO has high radiation hardness. All these properties make $Mg_xZn_{1-x}O$ a candidate for the deep ultraviolet photoelectric devices. In $Mg_xZn_{1-x}O$, the crystal lattice that has an Mg mole fraction between 37% and 62% is important to obtain (4.28-5.4 eV) band gap energies, that lead to obtain the solar blind region (220–280 nm) that can be used for the solar blind detectors. The defects within the MgZnO can impact on the optical absorption which changes the actual band gap and shifts the light absorption, such as oxygen vacancies which shift the optical absorption band from the deep ultraviolet region to the red region, this is reflected negatively on the performance of deep ultraviolet photoelectric devices [40].

3.4. MgZnO/ZnO Heterostructures

The heterostructures are quantum structures which composed of different materials which have different band gap to produce a quantum confinement of the carriers or the excitons. When we want to design devices based on heterostructures, we should pay attention to the band gap of each layer and the valence band as well as conduction band alignment between the individual layers [50]. In $Mg_xZn_{1-x}O$/ZnO heterostructures, the layers are strained, the effects of strain on the band structure should be known. The experimental studies use a chemical technique which is inconsiderate to the physical state of strain of heterostructures. In this state, first-principles calculations for $Mg_xZn_{1-x}O$ can be used to calculate effects of strain, bowing parameters, optical and electronic properties. There is a problem for $Mg_xZn_{1-x}O$/ZnO heterostructures with a high mole fraction of MgO, in which phase separation is expected.

For a moderate concentration of MgO (up to 37 %), $Mg_xZn_{1-x}O$ alloys have the wurtzite crystal structure of ZnO with a wide range of band gaps (3.37– 4.0 eV). As mentioned before, the Mg^{+2} (0.57Å) and Zn^{+2} (0.60Å) have a similar ionic radius, that makes the lattice without much distortion, that means the lattice for the $Mg_xZn_{1-x}O$ and ZnO matched enough to produce lattice matched confinement layers. Thus, $Mg_xZn_{1-x}O$ and ZnO can yield lattice-matched single-crystal heterostructures with polarization effects that happened at the interface layers. The carriers confine within the ZnO that act as a quantum well, whereas the $Mg_xZn_{1-x}O$ acts as a barrier layer, that lead to format two-dimensional electron gas where the carriers can move freely in the directions perpendicular to the growth direction but confined in the growth direction [51]. The quantum confinement phenomenon effect on the excitons within $Mg_xZn_{1-x}O$ /ZnO based quantum well heterostructures that reduce the exciton-phonon coupling. Thus, the excitons in the quantum well show a strong stability, which can be used in laser work and nonlinear absorption of II-VI-oxide quantum wells till at the room temperature. The carrier concentration and the mobility in the $Mg_xZn_{1-x}O$ /ZnO heterostructures change as the Mg mole fraction change. Also, they change according to the growth methods. In a high-quality $Mg_xZn_{1-x}O$ /ZnO heterostructures the carrier mobility can surpass 300 cm^2/V. S.

4. DENSITY FUNCTIONAL THEORY

In quantum mechanics, the wave functions contain a lot of information about a physical system. The Schrödinger equation can easily solve the wave equation of a simple physical system with one electron like Hydrogen.

In the case of many-electron systems, the Schrödinger equation becomes very complex and the wave function of the system can't be described easily by using it, that means Schrödinger equation is unable to describe how the quantum state of a quantum system changes through the time. So, the approximated method can be used to describe the many-electron systems such as *initio* method, Hartree-Fock theory and Monte Carlo methods [52].

The most common *initio* method is the density functional theory (DFT), which is classified as theoretical methods derived from fundamental equations, in which the properties of the many-electron systems can be described more easily such as the electronic properties, optical properties, vibrational properties, magnetic properties, the structures, etc. DFT can describe the properties of the metals and semiconductors bulk structures, as well as complex structures (such as protein) and nanostructure, etc. [53]

The basis of DFT is the Thomas-Fermi approximation, in which the main variable of the N-electron problem is the electron density. If the electron density has obtained, that's leading to determine both the Poisson potential and exchange-correlation components of the potential, this leads to the possibility the obtaining to a self-consistent solution. But the Thomas-Fermi is a simple approximation, can't do the material science and quantitative chemistry calculations accurately. So, theoretical studies on density functional theory have been carried out by Hohenberg-Kohn and Kohn-Sham, in which the ground state energy and the electron density were calculated instead of calculating wave function of many-electron systems [54].

The characteristics and behavior of a physical system can be obtained by solving the Schrödinger equation. The time-independent Schrödinger equation can be used for the nuclei and electrons system

$$\hat{H}\,\Psi(\,\vec{r}_1\,,\;\vec{r}_2\,...\,\vec{r}_n,\vec{R}_1\,,\vec{R}_2\,...\,,\vec{R}_N) = \hat{E}\,\Psi(\vec{r}_1\,,\;\vec{r}_2\,...\;\vec{r}_n,\vec{R}_1\,,\vec{R}_2\,...\,,\vec{R}_N) \qquad (4.1)$$

in which the $\hat{H}$ is the Hamiltonian operator, ψ is the wave function and E is the eigenvalue of the total energy. The electrons and nuclei can be described by the energies that pursue on them through the Hamiltonian operator $\hat{H}$ which utilized to determining the total energy of the particle system and can be defined as

$$\hat{H} = \frac{-\hbar^2}{2\,me}\,\sum_i \nabla_i^2 \;+\; \sum_{i,I}\frac{Z_I\,e^2}{|\vec{r}_i-\vec{R}_I|}\;+\;\frac{1}{2}\sum_{i\neq j}\frac{e^2}{|\vec{r}_i-\vec{r}_j|}\;-\;\sum_I\frac{\hbar^2}{2\,M_I}\nabla_I^2\;+$$

$$\frac{1}{2}\sum_{I\neq J}\frac{Z_I\,Z_J\,e^2}{|\vec{R}_I-\vec{R}_J|} \qquad (4.2)$$

where the *M, Z* and *R* indicate to the mass, charge and position of the nuclei, respectively. While the *m, e* and *r* indicate to the mass, charge and position of the electrons, respectively. The first term refers to the electrons nuclei kinetic energy, the second one refers to the attraction between electrons and nuclei, the third one refers to the repulsion between pairs of electrons, the fourth one refers to the nuclei kinetic energy and the fifth one refers to the repulsion between pairs of nuclei.

For real systems in which many particles interact to each together, solving this equation is very difficult and complex. Therefore, it is necessary to develop approximations to simplify the many-particle Schrödinger equation.

Because of the large value of the mass of the nuclei compared to the mass of the electron, therefore the electrons move faster than the nuclei. So, the fourth term can be considered small and can be ignored. This is an adiabatic approximation or the Born-Oppenheimer. It is a good approximation to the real systems that we talk about. So, the wave function of the System can be divided into electron's wave function and nucleus's wave function, as follows

$$\Psi(\vec{r},\vec{R}) = \;\Psi_{electron}(\vec{r},\vec{R})\;\;\Psi_{nucleus}(\vec{R}) \qquad (4.3)$$

The electron's wave function of the Schrödinger equation for a stable nucleus can be given as follows

$$\widehat{H}_{electron} \; \Psi_{electron}\left(\vec{r},\vec{R}\right) = E_{\;electron} \; \Psi_{electron}\left(\vec{r},\vec{R}\right) \tag{4.4}$$

In which $\Psi_{electron}\left(\vec{r},\vec{R}\right)$ is the electron's wave function and $\widehat{H}_{electron}$ is the Hamiltonian operator of the electron which can be written as

$$\widehat{H}_{electron} \; = \frac{1}{2}\sum_{i}\nabla_{i}^{2} \; - \sum_{i,I}\frac{Z_{I}}{|\vec{r}_{i}-\vec{R}_{I}|} \; - \sum_{i\neq j}\frac{1}{|\vec{r}_{i}-\vec{r}_{j}|} \tag{4.5}$$

The solutions of 4.4 and 4.5 equations give the total energy of the system. The Born-Oppenheimer approximation becomes applicable in the case of degeneration of the electronic state (or near degeneracy electronic states) [55].

4.1. Density Functional Approximation

A number of variables for both of wave function and electron density are the same regardless of the size of the system. Each different density produces different ground energy, but the functional that connects the density of the electron and ground energy was unknown. The goal of DFT is to find functional that connects the density of the electron and ground energy. The DFT is based on the proof of Hohenberg- Kohn theorem in which the ground state energy is determined by the electron density, as shown in the figure 4.1.
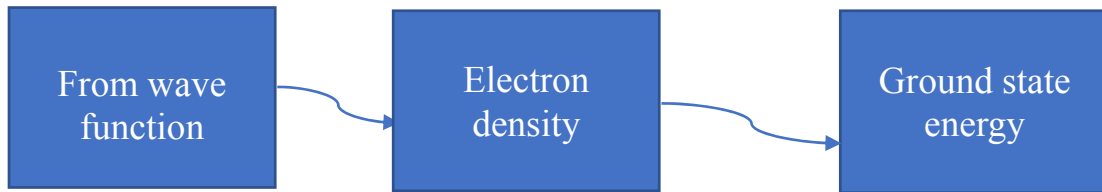

Figure 4.1. Illustration of the main idea of DFT

4.1.1. Hohenberg-Kohn theorem

The Hohenberg-Kohn theorem is modern theorem can be used to calculate the band structure of a system. It is the basis of DFT, in which the variable is the electron density [56].

The non-relativistic time-independent Hamiltonian of an N-particle system as given as follows,

$$\hat{H} = -\frac{1}{2} \sum_{i=1}^{N} \nabla_i^2 + \sum_{i=1}^{N} V(\vec{r_i}) + \sum_{i<j} \frac{1}{\vec{r}_{ij}} = \hat{T} + \hat{V}_{ext} + \hat{V}_{ee} \qquad (4.6)$$

Where the first term describes the kinetic energy, the second term describes the external forces that impacting the electrons and the last term describes the Coulomb effect between electrons. As it's known that the lowest energy of the system is the ground state energy. So, the electron density and the ground state energy can be obtained by determining the minimum of the energy functional which can be written as,

$$E_v[n] = \int v(\vec{r})n(\vec{r})d\vec{r} + F_{HK}[n] \qquad (4.7)$$

Where the $E_v[n]$ is the energy functional and the $F_{HK}[n]$ is a Hohenberg-Kohn functional that is a universal functional, which can be written as,

$$F_{HK} = < \Psi \mid \hat{T} + \hat{V}_{ee} \Psi > \qquad (4.8)$$

For an external potential, the variational principle exposure that,

$$E_0 < E_{v0} \qquad for \qquad n \neq n_0$$

$$E_0 = E_{v0} \qquad for \qquad n = n_0$$

Thus, ground state density can be obtained as follows,

$$E_0 = \min_{n} E_{v0}[n] \qquad (4.9)$$

The Hohenberg-Kohn theory is based on two theorems:

Theorem 1: The ground state energy is a functional of the electron density: *E=E[n(r)]*

Theorem 2: The electron density that minimizes the energy of the overall functional is the exact ground state electron density. *E[n(r)] > E₀[n₀(r)]*.

4.1.2. Kohn-Sham equations

The Kohn and Sham equations can be considered as a new description of the Hamiltonian in a simple arrangement with a changeable function that contribute to the realization of the Hohenberg and Kohn theorem. The Kohn and Sham equations are similar to the time-independent Schrödinger equation, but in Kohn and Sham equations the potential of the electron is given as a function of electron density [57].

The main idea of Kohn and Sham formalism is to divide the kinetic energy functional into two parts, the first term can be accurately calculated, and the second term is the correction term. The energy functional is written as

$$E[n] = \int v_{ext}(\vec{r})n(\vec{r})d\vec{r} + F \qquad (4.10)$$

$$F[n] = T[n] + U[n] + E_{ex}[n] \qquad (4.11)$$

where $T[n]$ is the kinetic energy functional, U $[n]$ is the electron-electron interaction functional and $E_{ex}[n]$ is exchange-correlation functional. The Kohn-Sham equations describe the particles that aren't interacting in the system. Thus, the Kohn-Sham equations explain accurately the many-electron system [57].

4.1.3. Local density approximation (LDA)

We need approximations that give correct results because the exchange-correlation energy is not known. The most common approximations are the LDA and the GGA. There are another functionals which derived from the LDA and GGA, which are Local-spin density approximation (LSDA), GGA+U and LDA+U, higher order gradient or meta-generalized gradient approximation (meta-GGA), etc.

The exchange-correlation energy functional can be approached as a non-local functional and a local functional. It can be divided into the exchange energy and the correlation energy. It can be written as,

$$E_{XC}[n] = E_X[n] + E_C[n] \qquad (4.12)$$

In the LDA, the density locally can be considered as a uniform electron gas that means the density varies slowly [58]. So, we can consider that there is a constant state at all points in the electron density. That means the Kohn-Sham equations uniform electron gas can be used,

$$E_{XC}[n] \approx E_{XC}^{LDA}[n] = \int n(\vec{r}) \, \varepsilon_{XC}^{hom}\big(n(\vec{r})\big) \, d\vec{r} \qquad (4.13)$$

This approximation can be used to describe the homogeneous systems and extended systems like metals.

4.1.4. Generalized gradient approximation (GGA)

The GGA functional can be used to improve the LDA approximation and to obtain more correct results than the LDA functional, especially for the inhomogeneous systems where the electron density locally changing. The gradient expansions approximation (GEA) has been inserted to the LDA functional to obtain the GGA functional where the electrons can be considered acting in a homogeneous system with values that change gradually. This approximation can give suitable results for the exchange energy but can't give good results for the correlation energy. So, for high-density systems, a good improvement can be obtained using GGA functional, but for low-density systems inaccurate description had been obtained. The generalized gradient approximation can be written as,

$$E_{XC}^{GGA}[n] = \int n(\vec{r}) \, \varepsilon_{XC} \, F_{XC}(\vec{r}_s, \vec{r}) d\vec{r} \qquad (4.14)$$

There are unwanted vibrations that can be removed using related exchange-correlation functionals which have been suggested by J. P. Perdew and colleagues. These functionals are PW86 (Perdew-Wang), PW91 (Perdew-Wang) and PBE (Perdew-Burke-Ernzerhof), which can be treated as improvements of the same pattern.

4.1.6. Hubbard term

Both LDA and GGA failed to yield accurate results for highly correlated systems that show strong effectiveness toward on-site Coulomb interaction such as transition metal oxides. Therefore, improvements can be made to these functionals by considering the on-site Coulomb interactions, where the orbital-dependent term can be inserted to the exchange-

correlation potential in LDA or GGA functionals to produce Hubbard correction which are indicated as XC+U, DFT+U, LDA+U, or GGA+U [59]. Hubbard correction is a semi-empirical correction that changes according to the studied system. The inserted orbital-dependent term can be written as,

$$E_U = \frac{1}{2} \sum_\mu U_\mu \ (n_\mu - n_\mu^2) \qquad\qquad (4.15)$$

where E_U is energy term, n_μ is the projection onto an atomic orbital and U_μ is the Hubbard for the orbital. If the orbital is a completely occupied or empty, the energy term is equal zero. Whereas the energy term takes a positive value for the partially occupied orbital. In this way, the energy is lowered if the levels are completely occupied or empty and the energy levels move far away from the Fermi level. So, the band gap increases, or the electrons are more localized if the broadening of states is reduced [60]. In this work, we will see how these functionals improved the results of electronic properties of wz-ZnO.

4.2. Quantum Methods

4.2.1. *Ab initio* method

The meaning of *ab-initio* is derived from "the first principles or the beginning". It is a method based on the quantum methods, which is theoretical methods derived from DFT and the Hartree-Fock self-consistent field (HF-SCF) methods, in which the properties of the large-scale atomistic systems can be calculated. In the HF-SCF method, Hartree suggested that the field that produced from the charge distribution should be self-constant, where the potential for electron-electron interactions is used to calculate the molecular structure and related properties. The properties of wide-band gap systems can be calculated by *ab-initio* methods [61].

4.2.2. Pseudopotential method

The pseudopotential method is a theoretical method that is an extension of the orthogonalized plane-wave (OPW) method. In the pseudopotential method, the total wave function is divided into two parts which an oscillatory part and a smooth part, which can be called pseudo wave function. The pseudopotential method is so-called frozen core method,

that's mean the core electrons can be ignored (they can be frozen) because the calculation will be more expensive due to core electrons. Therefore, a weaker potential valid for the valence electrons is obtained instead of the strong exact potential [62].

4.2.3. Linear combination of atomic orbitals (LCAO)

The linear combination of atomic orbitals (LCAO) is a theoretical method based on density functional theory where the linear combination of atomic orbitals is used. The main idea of the LCAO method is to find a variational solution where the wave function consists of linear combination orbitals of isolated atoms and use this solution in the Schrodinger equation to calculate new eigen energies [63].

5. CALCULATION METHODS AND MODELS

The ZnO structures and $Mg_xZn_{1-x}O$/ZnO heterostructures are very important materials due to their applications in electronic and electro-technology industries, photovoltaic devices, etc. $Mg_xZn_{1-x}O$ /ZnO heterostructures and ZnO structures can be grown using different methods such as chemical vapor deposition (CVD), plasma-enhanced chemical vapor deposition (PECVD), expanding thermal plasma, vacuum arc deposition and vacuum sputtering. To obtain high-quality crystals and develop their applications, many experimental studies have grown ZnO and $Mg_xZn_{1-x}O$/ZnO heterostructures using different methods under different growth conditions such as different pressures and different temperatures. The experimental studies are unfocused on the physical state of structures. So, the first-principles calculations for MgZnO can be used to calculate the effects of strain, optical and electronic properties, etc.

In this thesis, the electronic and optical properties of wz- $Mg_xZn_{1-x}O$ structures were investigated with the help of DFT. To understand the changes in the optical and electronic properties of wz- $Mg_xZn_{1-x}O$, it is necessary to study the effects of Mg on those properties by increasing the Mg mole fraction in the ZnO structures, including the band structures, density of states, electron effective masses, dielectric functions, refractive indexes, extinction coefficients and absorption spectra. So, the DFT, in which the electronic interactions are defined within the GGA + U formalism, was used.

5.1. Previous Studies on Wurtzite ZnO

As mentioned earlier, LDA and GGA functionals had given inaccurate results. Therefore, some of these studies used the meta-GGA functional, whose results of electronic properties were better than the LDA and GGA, but the results for the optical properties were underestimated the complex dielectric constant, refractive index, extinction coefficient and absorption coefficients [13]. Some of these studied used GGA+U (or LDA+U) functionals, in which the results of electronic and optical properties were close to the experimental results [13-14].

In ZnO, there is a strong hybridization between the Zn-3d electrons with O-2p electrons. The LDA, GGA and meta-GGA ignored that hybridization. So, to describe this hybridization, the hybrid functionals should be used, in which Hubbard parameters were taken in consideration, consequently, these functionals overcome the underestimation of band gaps and give accurate results for electronic and optical properties of $Mg_xZn_{1-x}O$.

Few of the theoretical investigations focused on the effects of Hubbard parameters and effects of changes in values of Hubbard parameters on the related properties of ZnO. They made one of the Hubbard parameters fixed and changed the other one, as shown in figure 5.1. However, the band gap values still small. They changed the both of Hubbard parameters and good band gap values were obtained [13].
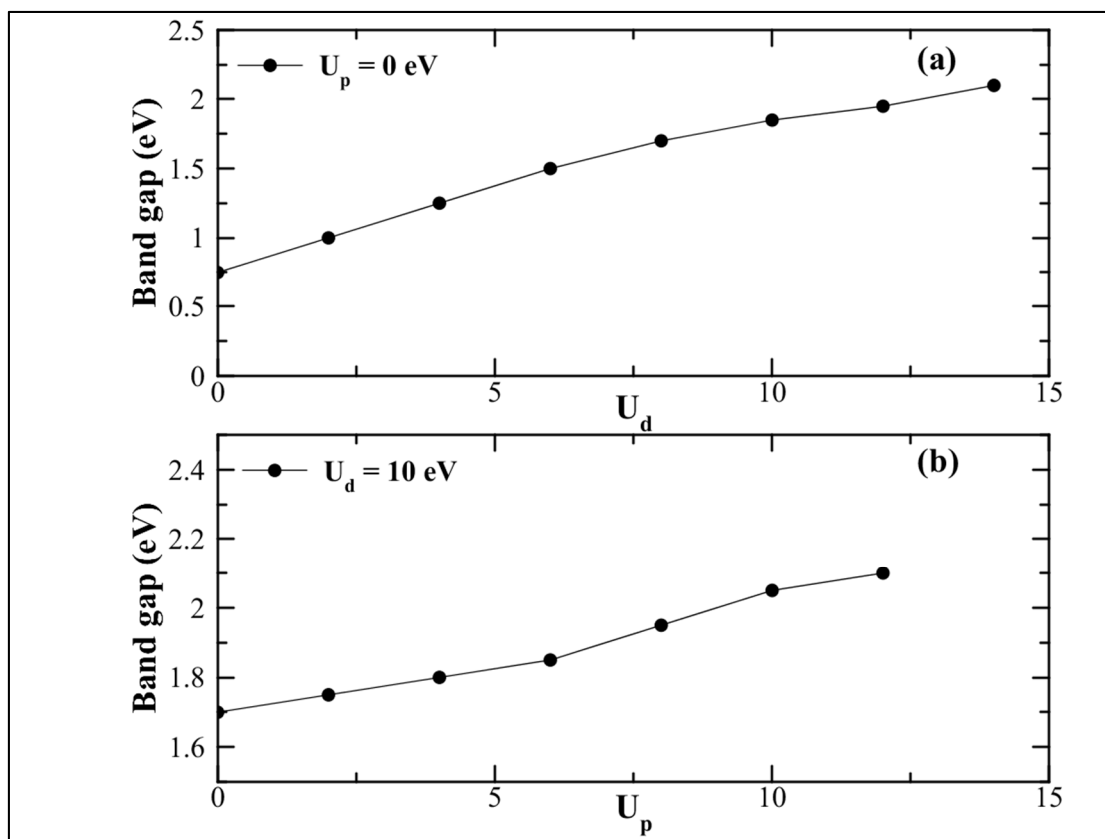

Figure 5.1. The band gap of ZnO as a function to (a) Hubbard U of Zn-3d and (b) Hubbard U of O-2p

In some investigations, the values of the Hubbard parameters that gave accurate results for the band gap, were almost similar. Where Xinguo Ma *et al.* found that the best Hubbard parameters were $U_{O-2P} = 7$ eV and $U_{Zn-3d} = 10$ eV [12], in Qiao Liping *et al.* investigation they were $U_{O-2P} = 7.1$ eV and $U_{Zn-3d} = 10.57$ eV [41] and Sheez *et al.* investigation they were

U_{O-2P} = 7 eV and U_{Zn-3d} =10 eV [64]. While BAI Li-Na *et al*. found that the U_{O-2P} = 8 eV and U_{Zn-3d} = 4.5 eV were the best Hubbard parameters [14].

5.2. Calculation Details for wz-ZnO

Initially, the optical and electrical properties of pure wz-ZnO were calculated. The calculations were performed using the Atomistic Toolkit-Virtual Nano Lab (ATK-VNL) software based on DFT.

In our calculations, the lattice parameters were *a* = 0.32491 Å and *c* = 0.52042 Å [65], the ratio between the lattice parameters *c/a* is equal 1.602. The super cell was built as 2×2×2 where the number of atoms was 32 which 16 of them are Zn atom and 16 O atoms. The hybrid-generalized gradient approximation (GGA+U) was used. The effect of hybridization is applied to 3d Zn electrons and 2p O electrons. The Hubbard parameters that gave accurate results were U_{O-2P} = 7 eV and U_{Zn-3d} =10 eV [42]. The mesh cut-off energy was 500 eV. The 6×6×5 k-points were used and a broadening of 0.1 eV is applied. Figure 5.2 shows the crystal structure for wz-ZnO.

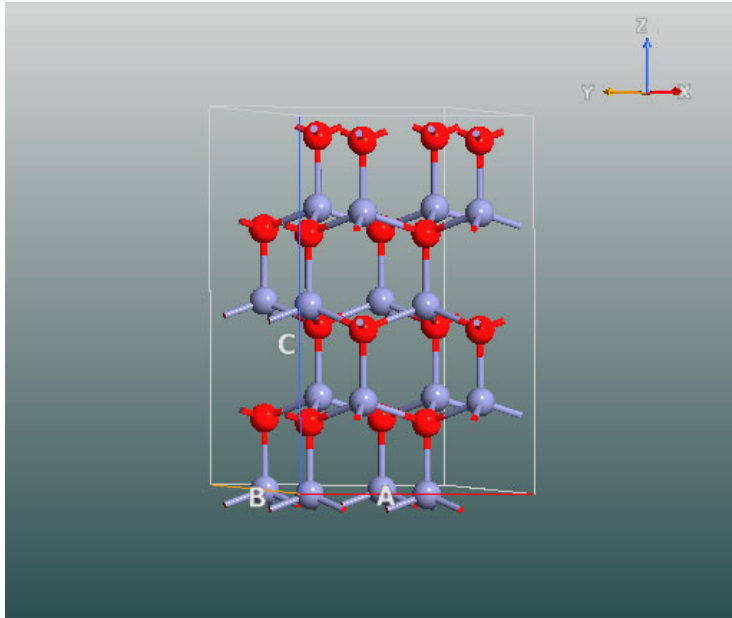Figure 5.2. The crystal structure of the 2×2×2 super cell of wz-ZnO, where the red and purple balls represent O and Zn atoms, respectively

5.2.1. Electronic properties for wz-ZnO

The electronic properties allow us to understand the band structures and know the band gap values. Consequently, the type of materials can be determined. In addition, orbitals that contribute in the valence band and the conduction band can be determined.

Figure 5.3 shows the band structure of wz-ZnO. It is clear that ZnO has a direct band gap as long as the both the VBM and the CBM are situated at Γ point, as mentioned previously. The VBM located at -2.87 eV and the conduction band minimum located at 0.48 eV. Thus, band gap energy is equal to 3.35 eV, which is very similar to the results that found in the literature [12]. That means wz-ZnO is a wide band gap semiconductor. The Fermi level located at 0 eV, which is the highest state of energy that electrons occupy in a material at absolute zero temperature. The location of the Fermi level can be changed due to the alloying, presence of impurities and change in temperature.
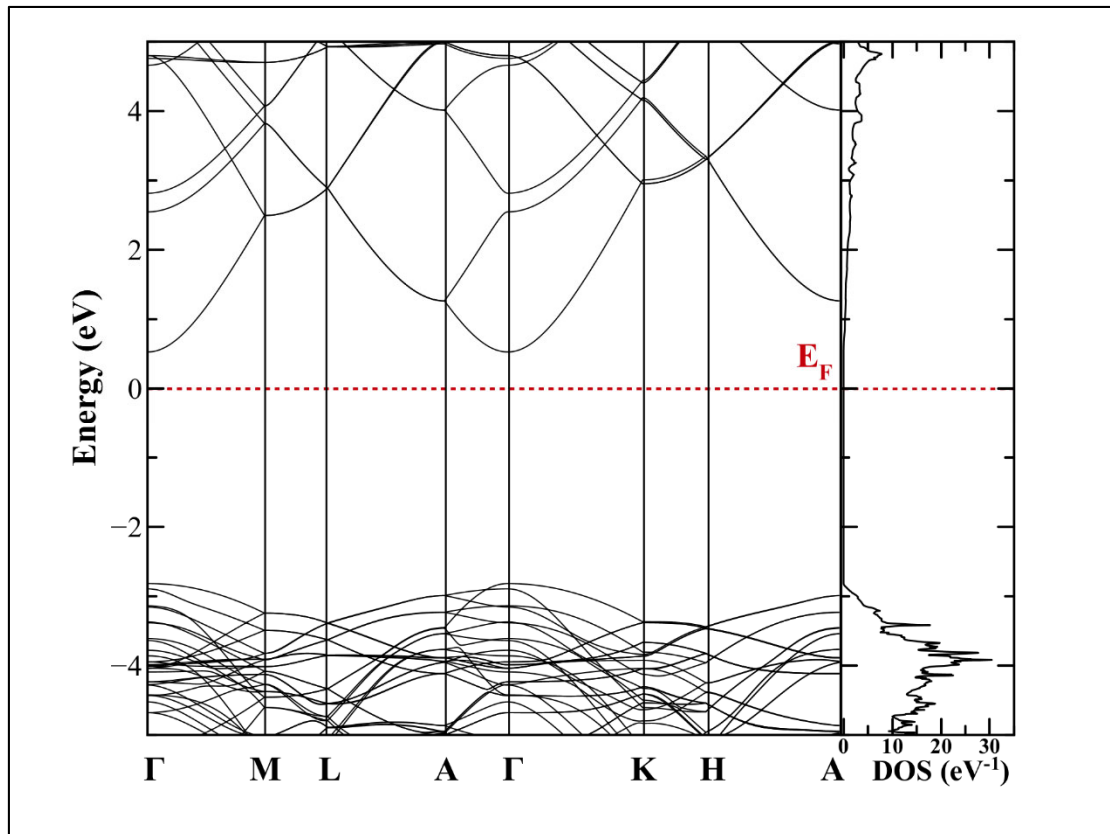

Figure 5.3. The band structure and density of states of pure wz-ZnO

The figure 5.4 shows the total density of state of wz-ZnO and the partial densities of states of Zn and O atoms. Both of O_{2p} state and Zn_{3d} state primarily contributed in the valence band which ranges between -2.87 eV and -12 eV. In addition, the O_{2s} state contributed in the lower part of valence band which ranges between -17 eV and -18 eV, but this part does not appear in this figure. The hybridization of the Zn_{3d} state with the O_{2p} state is clear from their contribution in the valence band. While, the Zn_{4s} state primarily contributed to the conduction band which ranges between 0.48 eV and 15.5 eV. The O_{2p} and O_{2s} states also contributed in the conduction band but the contribution is smaller than Zn_{4s} state.
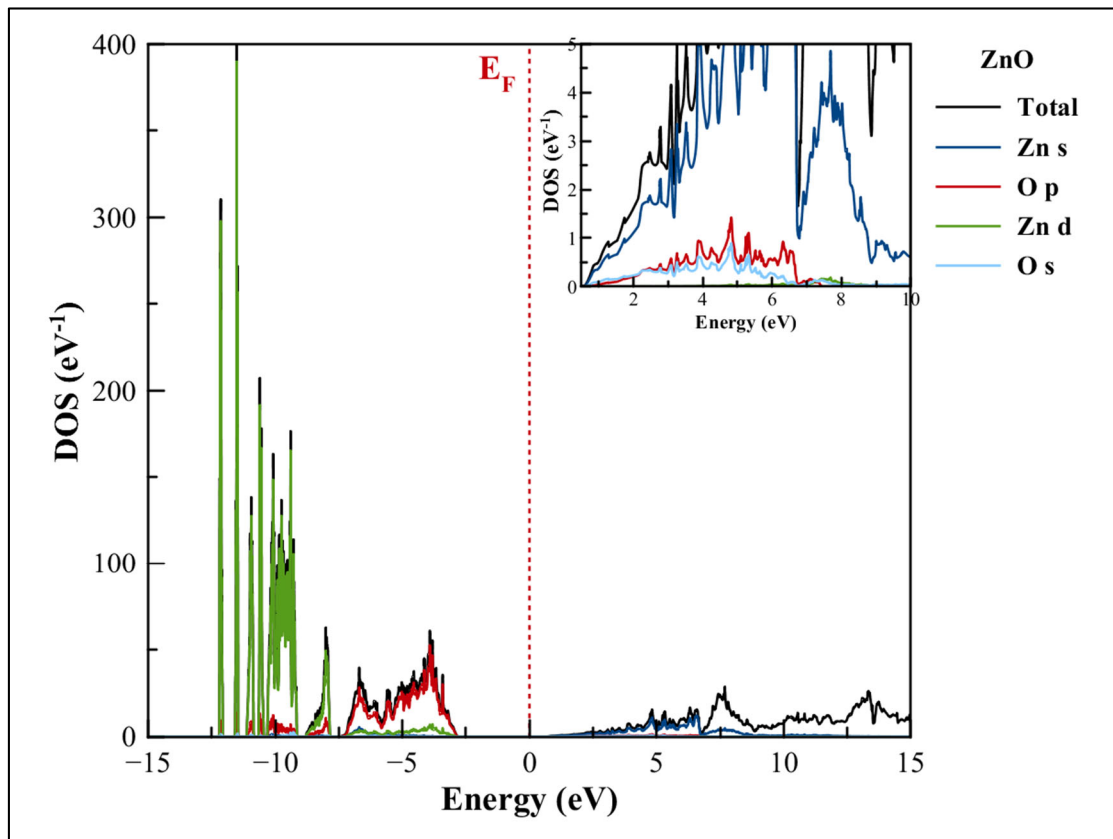

Figure 5.4. The details of the density of states of pure wz-ZnO

The electron effective mass of wz-ZnO was calculated which was equal to 0.383. It was bigger than its value reported in literature studies [43].

5.2.2. Optical properties for wz-ZnO

It is very necessary to study the optical properties of a material such as of the dielectric function, the refractive index, the extinction coefficient and the absorption coefficient. For wz-ZnO, these optical properties are anisotropic due to the difference in lattice parameters. Where, these optical properties are isotropic for the perpendicular directions on the *c* axis, where the lattice parameters *a* and *b* are equals. So, their optical characteristics are similar to each other and dissimilar to the c axis optical characteristic.

Figure 5.5 shows the real part and imaginary part of the dielectric function of pure wz-ZnO. There is no absorption for energy values below the energy gap where the electron can't be present. That means, for the energies smaller than the band gap, the real part of the dielectric function has a smooth dispersion. There is a slow increase in the real part of the dielectric function. For ε_{1XX} and ε_{1YY}, when photon energy increases from 0 eV to 3.35 eV, the real part increases slowly from 2.99 to 3.07. But for ε_{1ZZ} the real part increases slowly from 3.07 to 4.32 when photon energy increases from 0 eV to 3.35 eV. There is a peak for the both ε_{1XX} and ε_{1YY}, that is equal to 4.46 at 3.8 eV. For ε_{1ZZ}, this peak is equal to 4.84 at 3.6 eV. The imaginary part remains negligible until 3 eV and then starts to change randomly up to the peak that is equal to 2.63 at 4.45 eV for the ε_{2XX} and ε_{2YY}, whereas for the ε_{2ZZ} the peak is equal to 2.25 at 4.85 eV. Some of the experimental investigations reported both the real part and the imaginary part of the dielectric constant of wz-ZnO, where was equal to 3.7 and 2.5 at 3.4 eV, respectively [66].
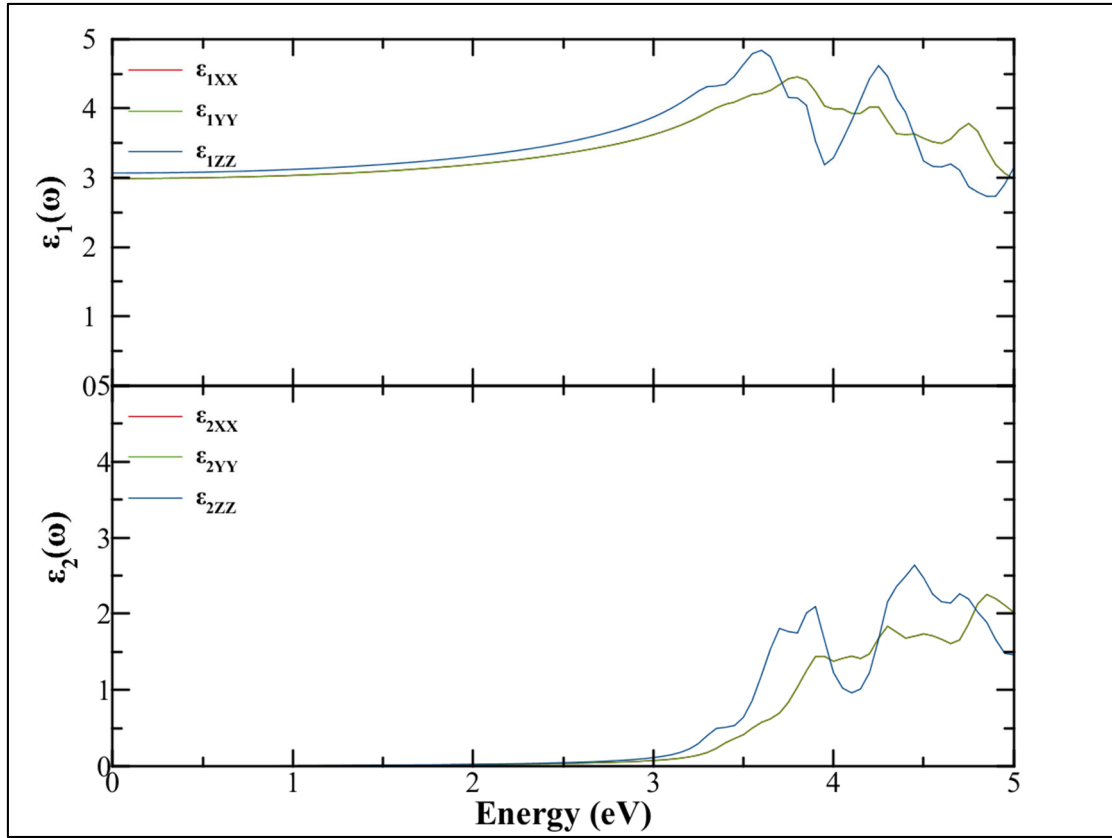
Figure 5.5. The dielectric function of pure wz-ZnO

Figure 5.6 shows the refractive index as a function of energy. There are two peaks, for n_{ZZ}, the peaks are (2.22 and 2.18) which corresponds to energies (3.6 and 4.25) eV. While for n_{XX}, the peaks are (2.13 and 2.05) which corresponds to energies (3.8 and 4.25) eV. They are larger than the results that can be found in the literature [39].
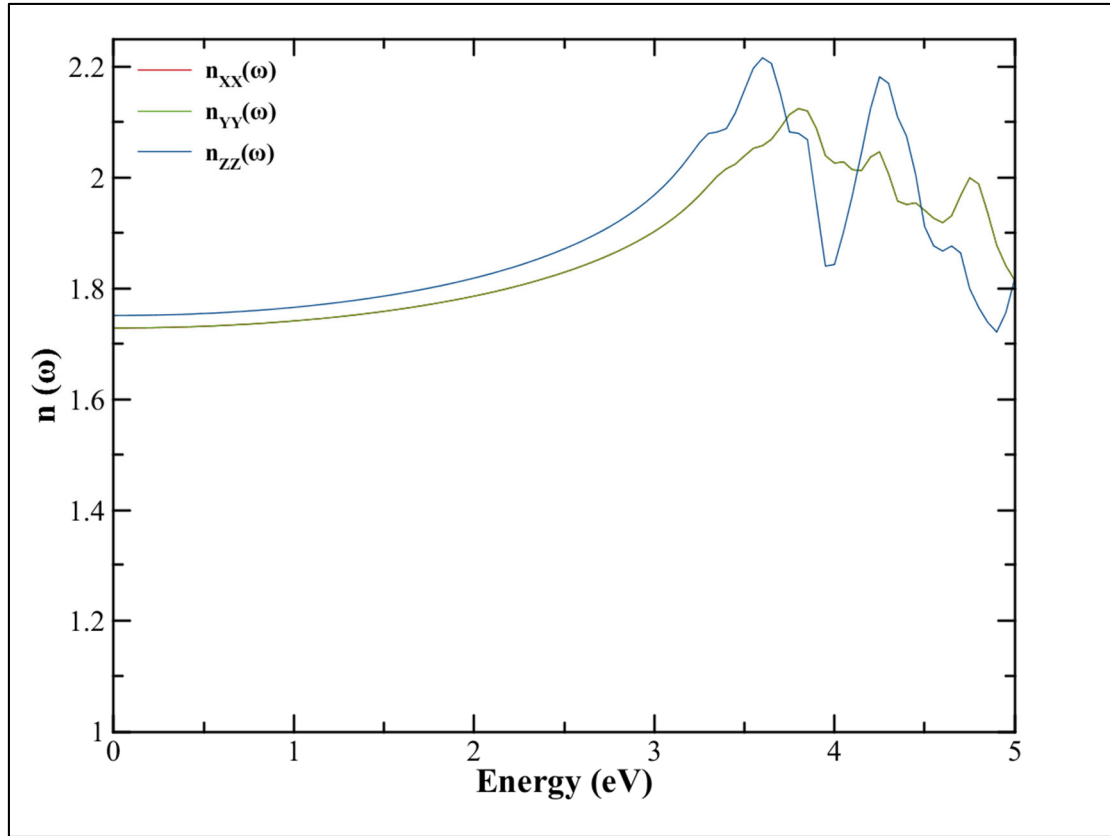
Figure 5.6. The refractive index of pure wz-ZnO

For example, the peak of the refractive index was 2.06 at 2.55 eV. Both the real part of the dielectric function and the refractive index has the same dependence on energy.

Figure 5.7 shows the extinction coefficient as a function of energy. There are two peaks, for n_{ZZ}, the peaks are (0.54 and 0.66) which corresponds to energies (3.9 and 4.45) eV. While for n_{XX}, the peaks are (0.46 and 0.59) which corresponds to energies (4.3 and 4.9) eV. They are close to the results that can be found in the literature [13].

Figure 5.8 shows the absorption coefficient as a function of energy, as can be seen, the absorption coefficient values are ignored up to 3.35 eV, where no absorption occurs which corresponds to the band gap value where the electron is not present. There are two main peaks (21.10 and 29.51) $\times 10^6$ m^{-1} at (3.9 and 4.45) eV. These values are larger than the results that can be found in the literature [14].
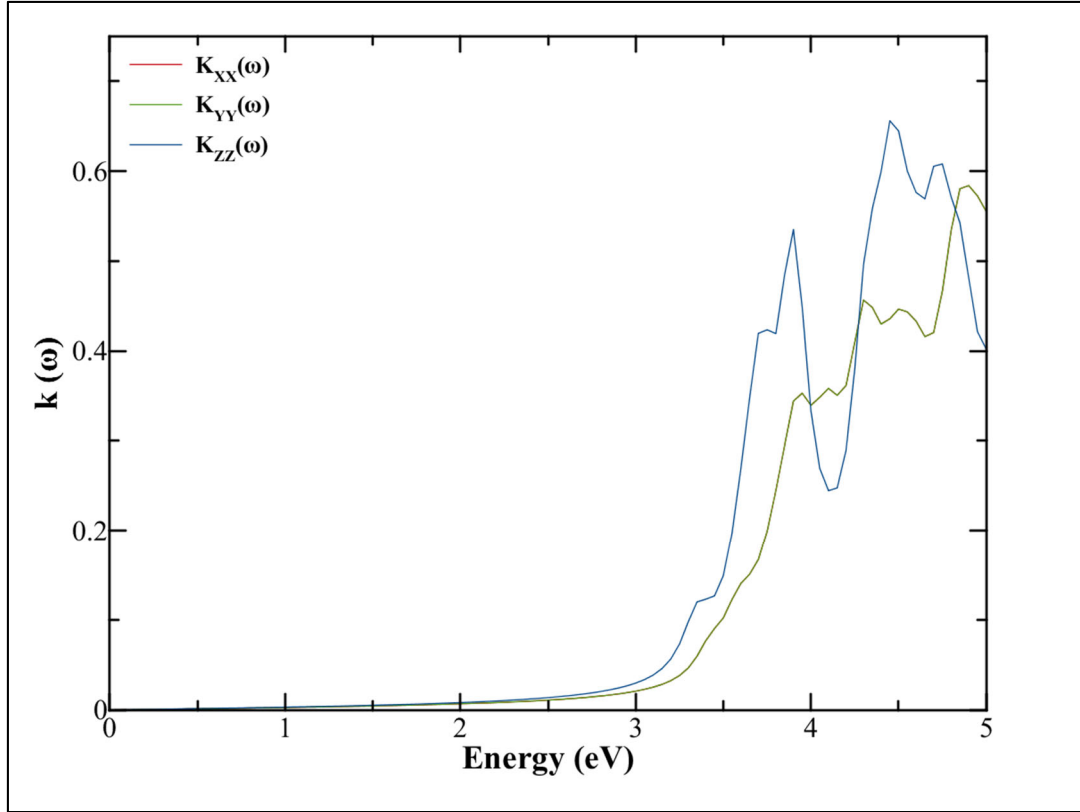
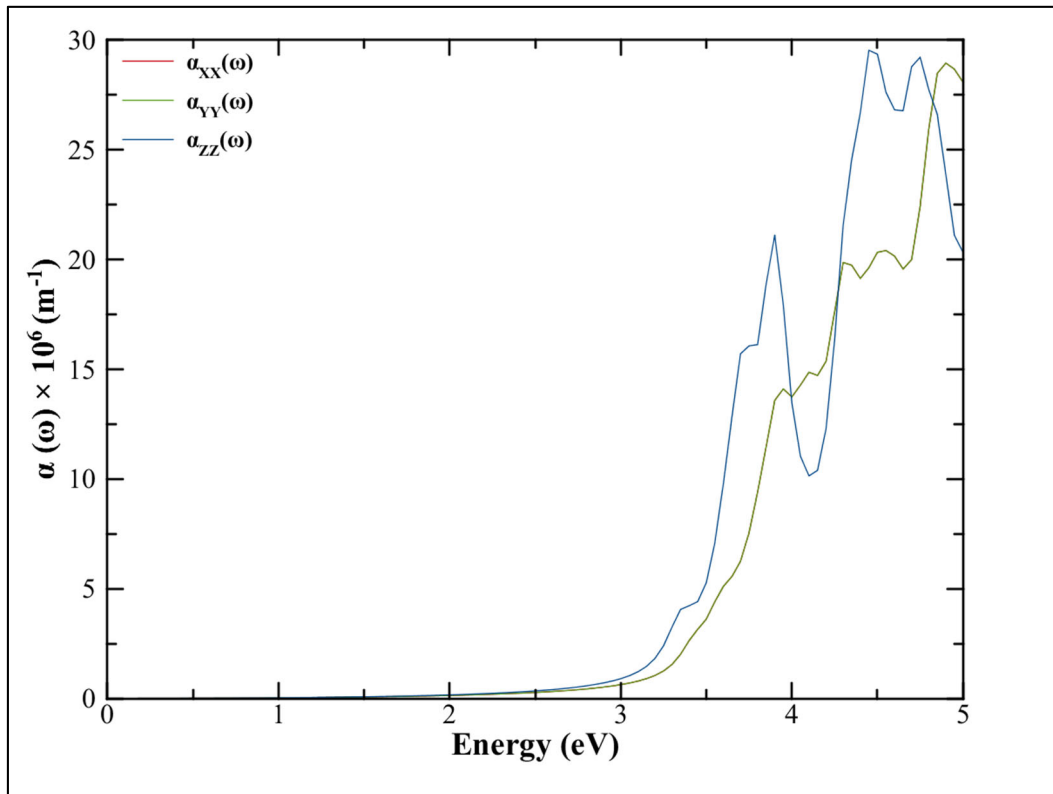Figure 5.7. The extinction coefficient function of pure wz-ZnO

Figure 5.8. The absorption coefficient function of pure wz-ZnO

All the imaginary part of the dielectric function, the absorption coefficient, and the extinction coefficient have the same dependence on energy.

5.3. Calculation Details for wz- $Mg_xZn_{1-x}O$

In MgZnO calculations, the optical and electrical properties of wz-$Mg_xZn_{1-x}O$ were calculated for (6.25%, 12.5%, 18.75%, 25% and 31.25%) Mg mole fractions. In the optimization calculations, experimental lattice parameters for $Mg_xZn_{1-x}O$ crystal were used as $a = b = 0.32491 + 0.047\,x$ and $c = 0.52042 - 0.072\,x$ [68]. The calculations were performed using the ATK-VNL software based on DFT. The super cell was 2×2×2. The GGA+U was used. The Hubbard parameters were $U_{O-2P} = 7$ eV and $U_{Zn-3d} = 10$ eV. The mesh cut-off energy was 500 eV. The 6×6×5 k-points were used and a broadening of 0.1 eV is applied. Magnesium positions were randomly selected several times, where the results of all calculation were close enough. $Mg_xZn_{1-x}O$ super cell were structurally optimized under an analytic potential [66]. The figure 5.9 shows the crystal structure for wz-$Mg_{0.3125}Zn_{0.6875}O$, where the red, purple and green balls represent O, Zn and Mg atoms, respectively.
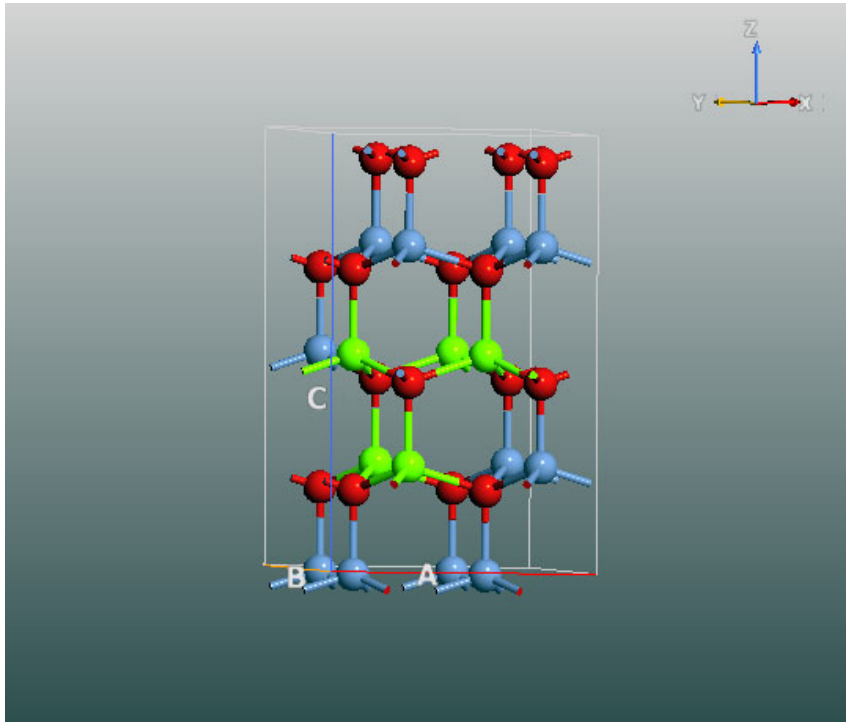

Figure 5.9. The crystal structure of the 2×2×2 super cell of wz-$Mg_{0.3125}Zn_{0.6875}$

5.3.1. Electronic Properties

The electronic properties allowed us to understand the change in the band structures of wz-ZnO and how the band gap values changed when Mg mole fractions changed. The effect of magnesium on the density of state of wz-ZnO and the partial densities of states of Mg were obtained. In addition, the electron effective masses of wz- $Mg_xZn_{1-x}O$ were determined.

Figures 5.10, 5.11, 5.12, 5.13 and 5.14 show the band structures of wz-$Mg_xZn_{1-x}O$ for different Mg mole fractions (6.25%, 12.5%, 18.75%, 25% and 31.25%), respectively. It is clear from the figures that wz-MgZnO has a direct band gap as long as both the VBM and the CBM are located at Γ point, where the CBM located at 0.48 eV and the VBM located at (3, 3.11, 3.22, 3.31 and 3.38) eV, respectively. Thus, wz-$Mg_xZn_{1-x}O$ O is a wide band gap semiconductor such as wz-ZnO.
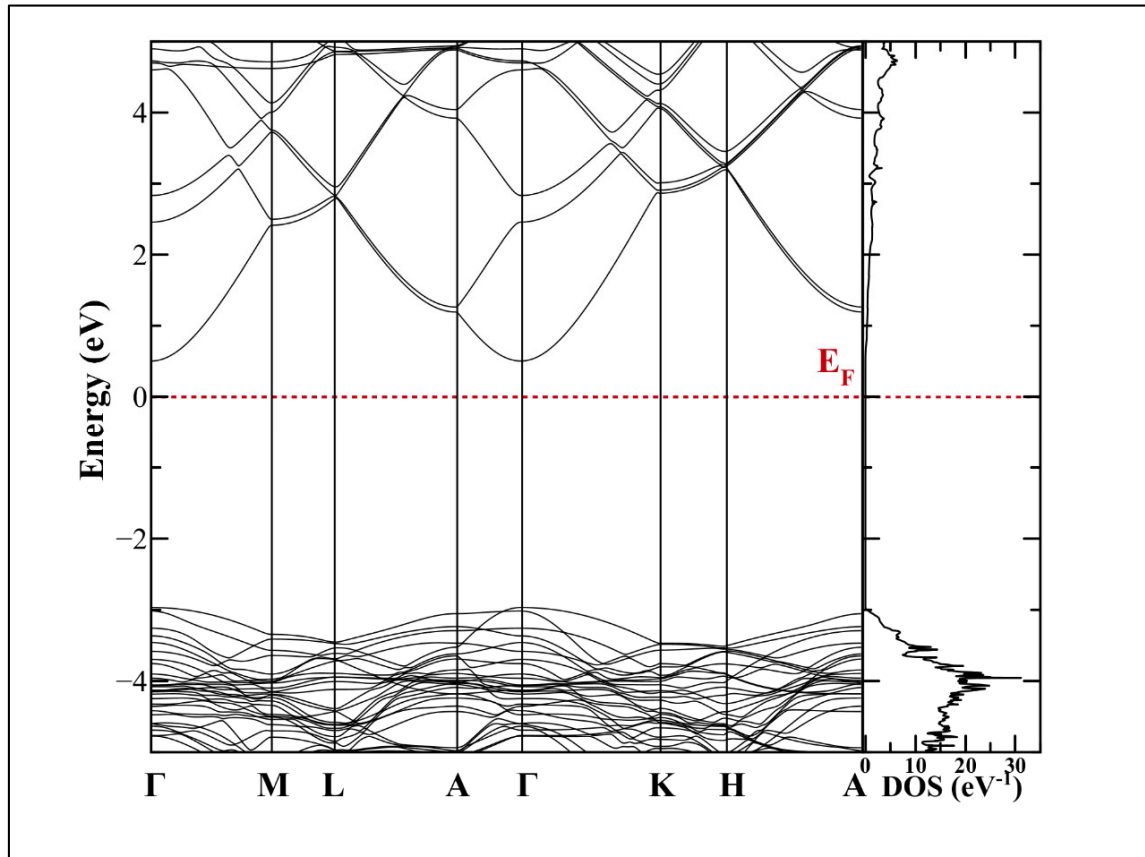

Figure 5.10. The band structure and density of states wz-$Mg_{0.0625}Zn_{0.9375}O$

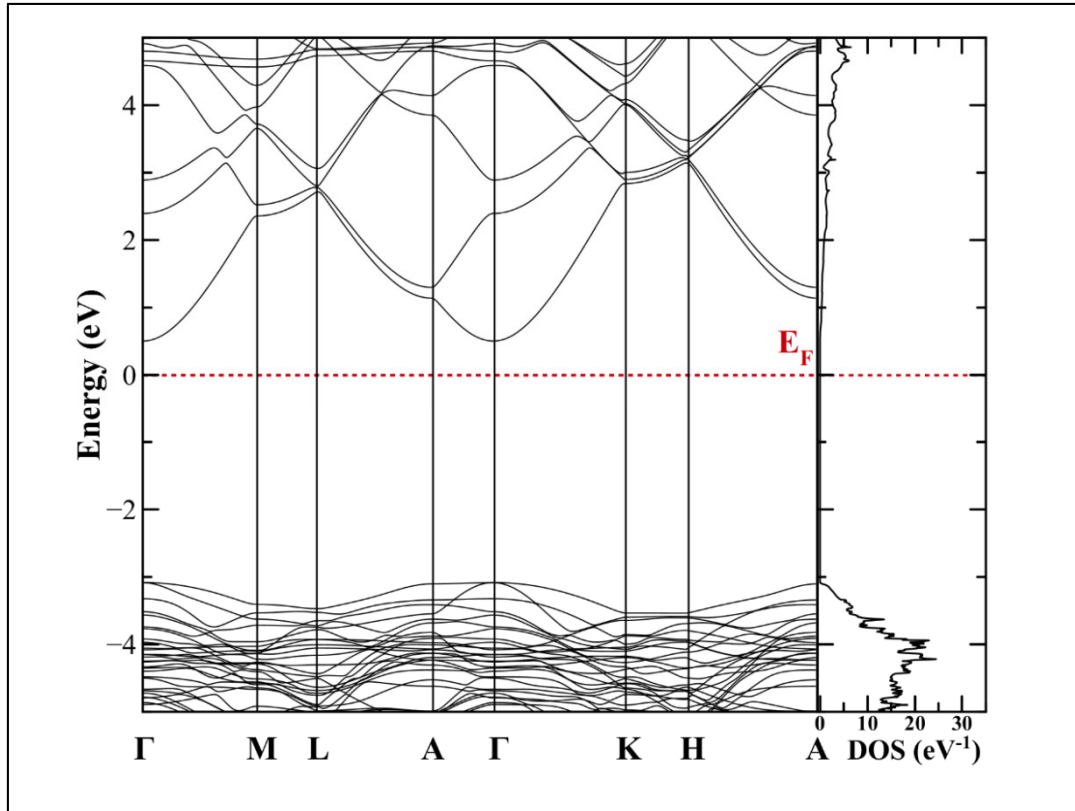Figure 5.11. The band structure and density of states wz-$Mg_{0.125}Zn_{0.875}O$

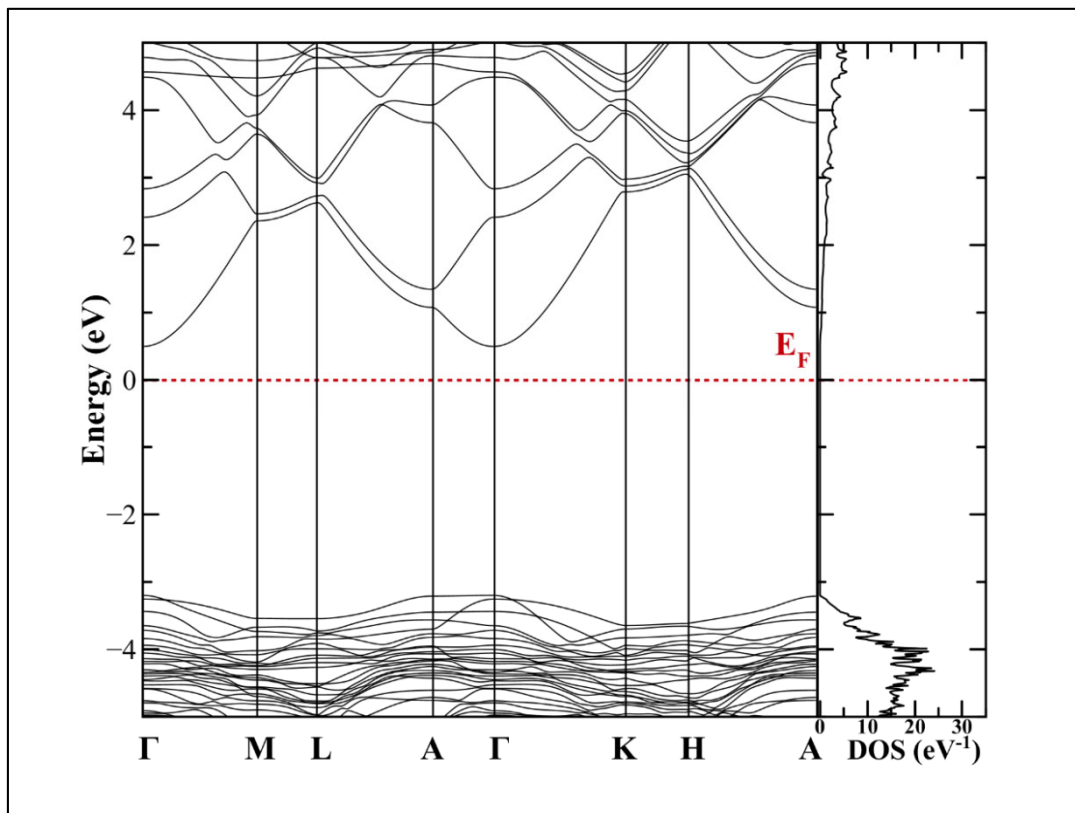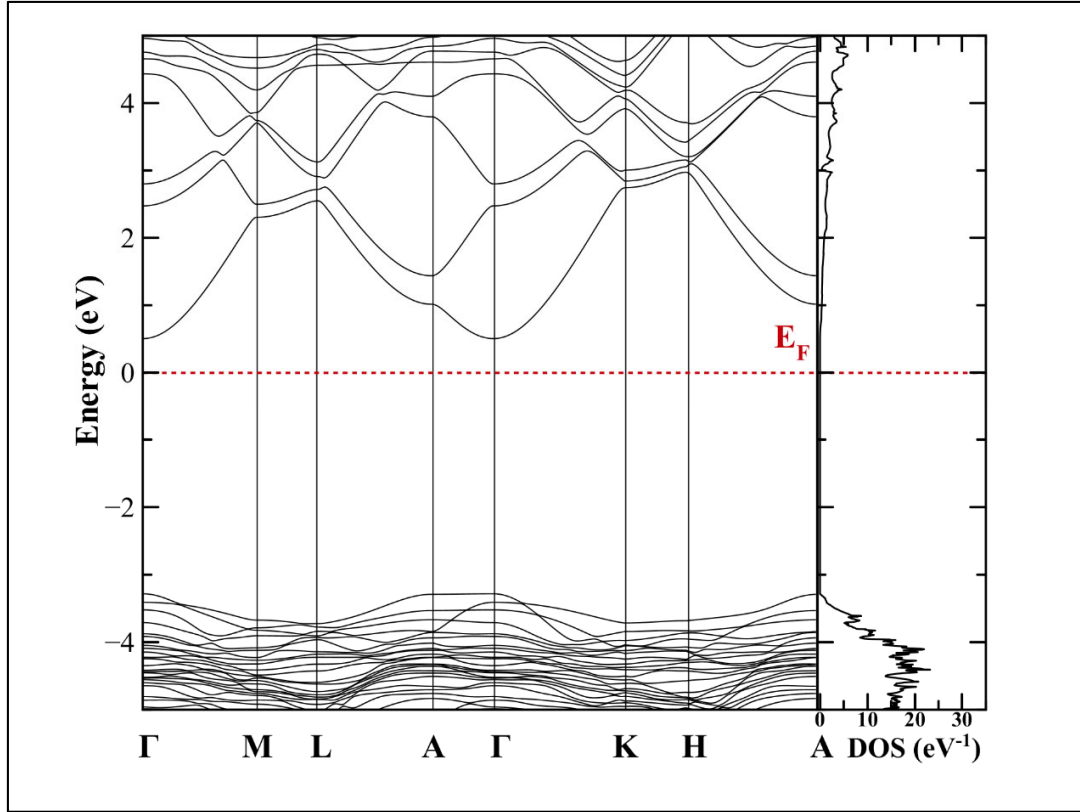Figure 5.12. The band structure and density of states wz-$Mg_{0.1875}Zn_{0.8125}O$

Figure 5.13. The band structure and density of states wz-$Mg_{0.25}Zn_{0.75}O$
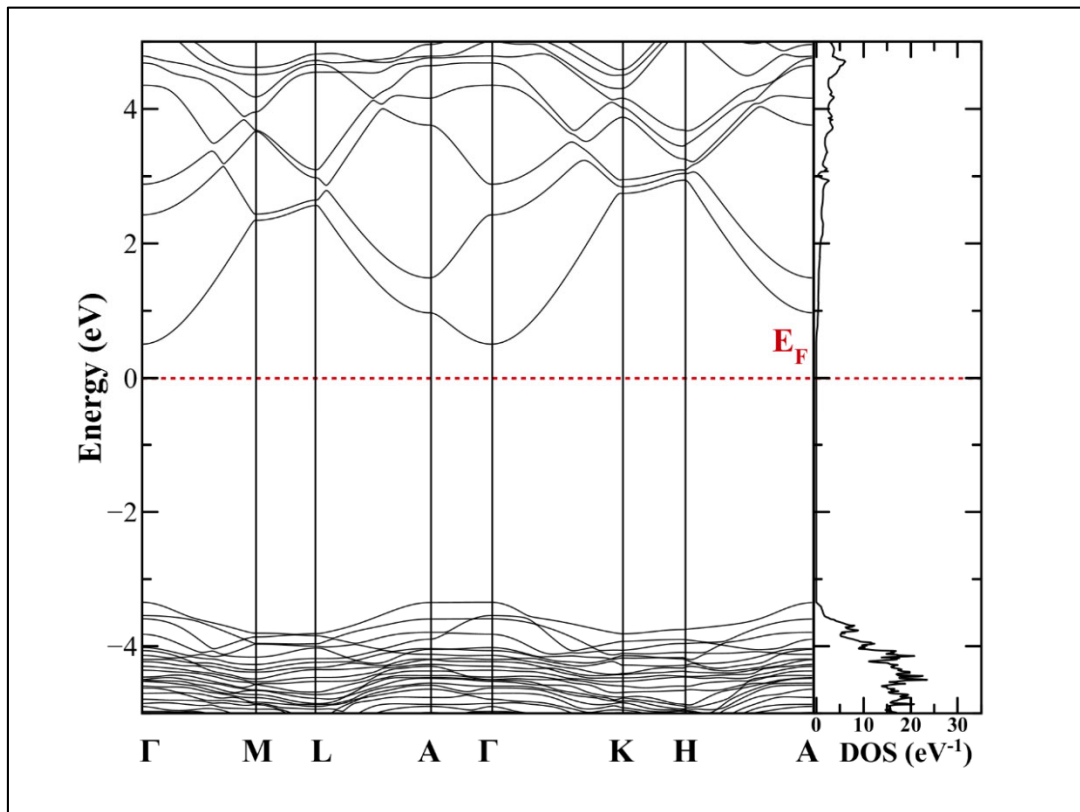

Figure 5.14. The band structure and density of states wz-$Mg_{0.3125}Zn_{0.6875}O$
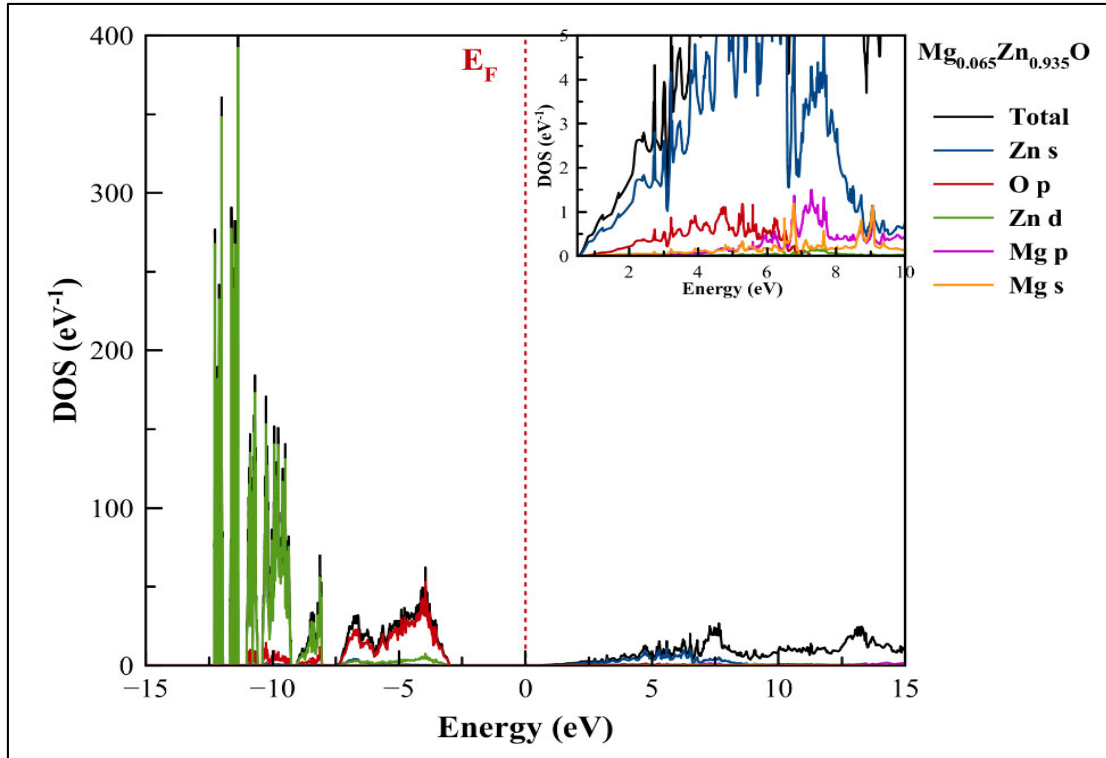
Figure 5.15. The partial density of states wz-Mg$_{0.0625}$Zn$_{0.9375}$O

Figure 5.16. The partial density of states wz-Mg$_{0.125}$Zn$_{0.875}$O

Figure 5.17. The partial density of states wz-Mg$_{0.1875}$Zn$_{0.8125}$O

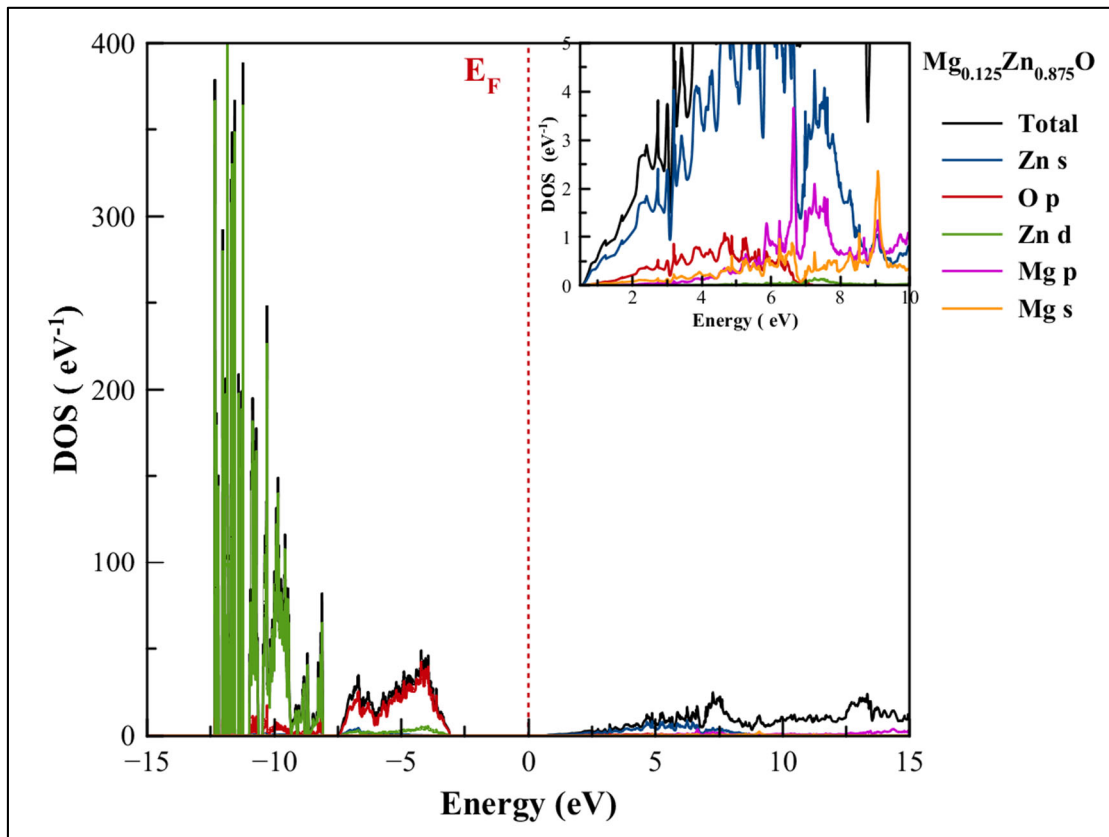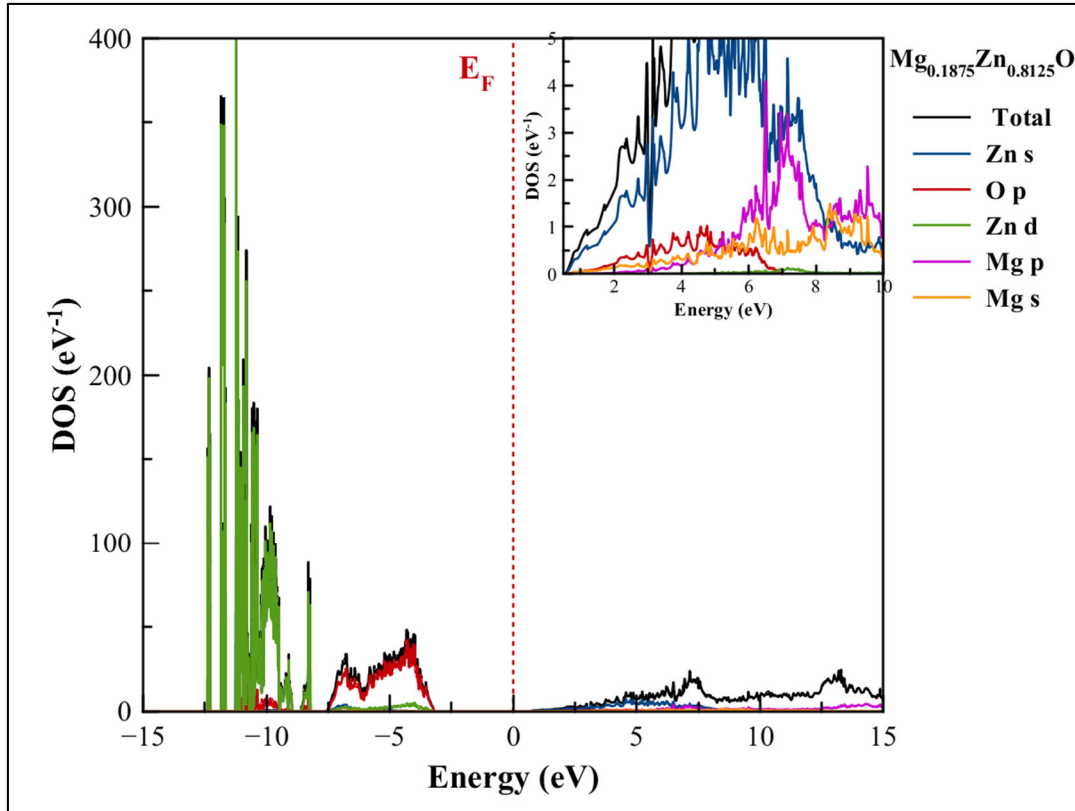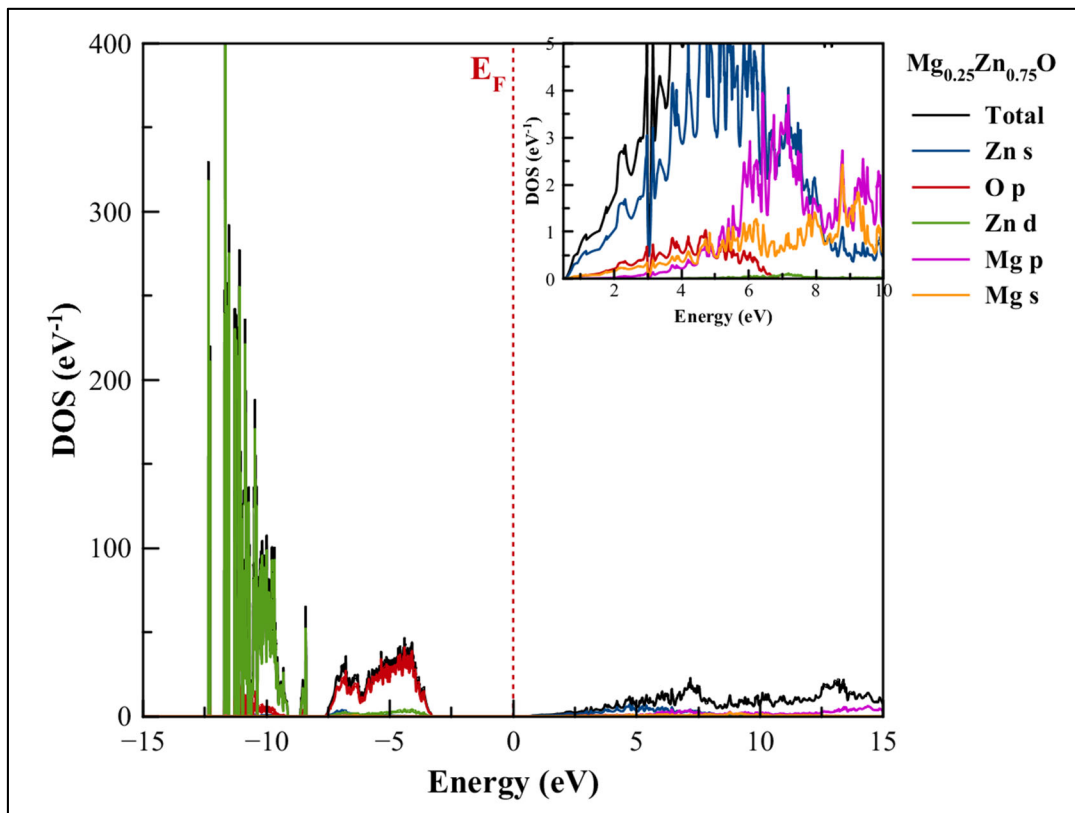Figure 5.18. The partial density of states W-Mg$_{0.25}$Zn$_{0.75}$O
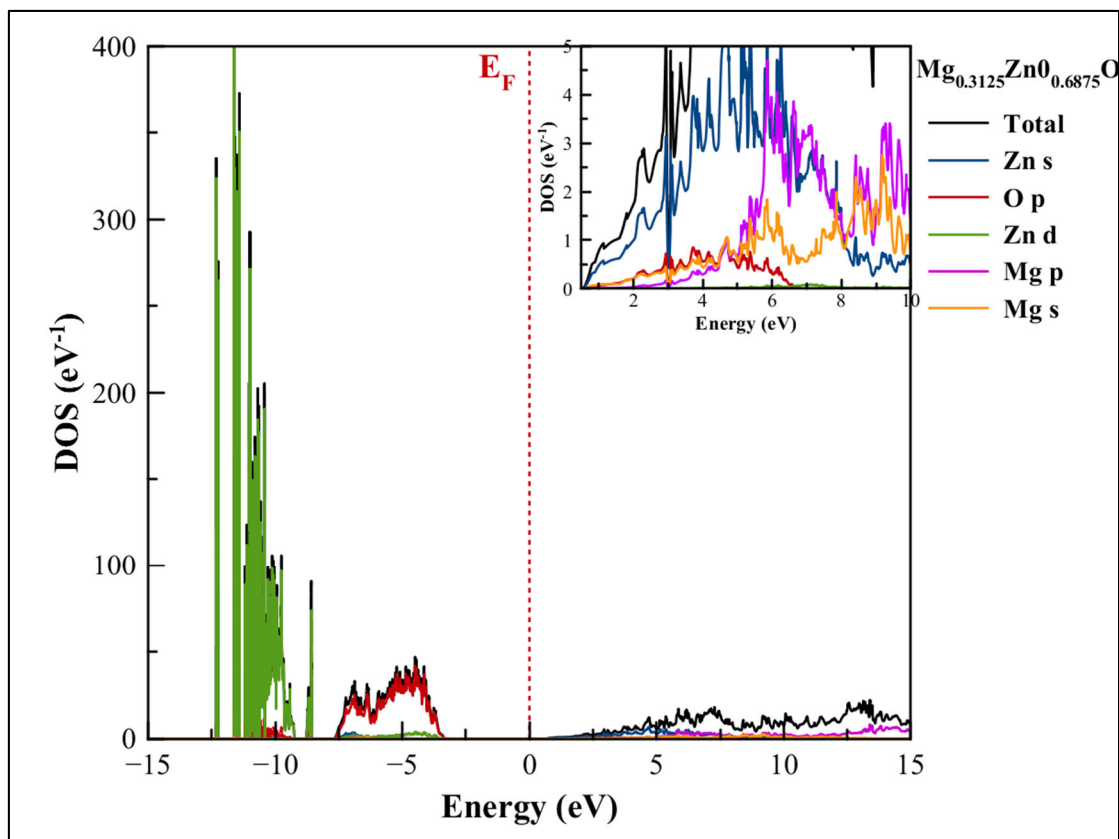
Figure 5.19. The partial density of states W-Mg$_{0.3125}$Zn$_{0.6875}$O

The figures 5.15, 5.16, 5.17, 5.18 and 5.19 show the partial densities of states of Zn, O and Mg atoms for wz-Mg$_x$Zn$_{1-x}$O. Both of O$_{2p}$ states and Zn$_{3d}$ states primarily contributed in the valence band which range from (-3, -3.11, -3.22, -3.31 and -3.38) eV to -12 eV, respectively. In addition, the Mg$_{3s}$ and Mg$_{2p}$ states slightly contributed in the valence band. While the Zn$_{4s}$ state primarily contributed to the conduction band which ranges between 0.48 eV and 15.5 eV. The O$_{2s}$, Mg$_{2p}$ and Mg$_{3s}$ states also contributed in the conduction band but its contribution is smaller than Zn$_{4s}$ state. As can be seen from the figures, that the Mg$_{2p}$ and Mg$_{3s}$ state's contribution to the conduction band increase with the Mg mole fraction increase. The Zn$_{3d}$ state contribution in the valence band becomes denser with the Mg mole fraction increases.

The figure 5.20 shows the partial densities states of Mg, where the CBM stay at the same position but the VBM position slightly changes with Mg mole fraction change. But the VBM position is not clear enough to discuss in the figure 5.20.

Figure 5.20. The partial densities states of Mg

Figure 5.21. The partial densities states in the valence band of Mg

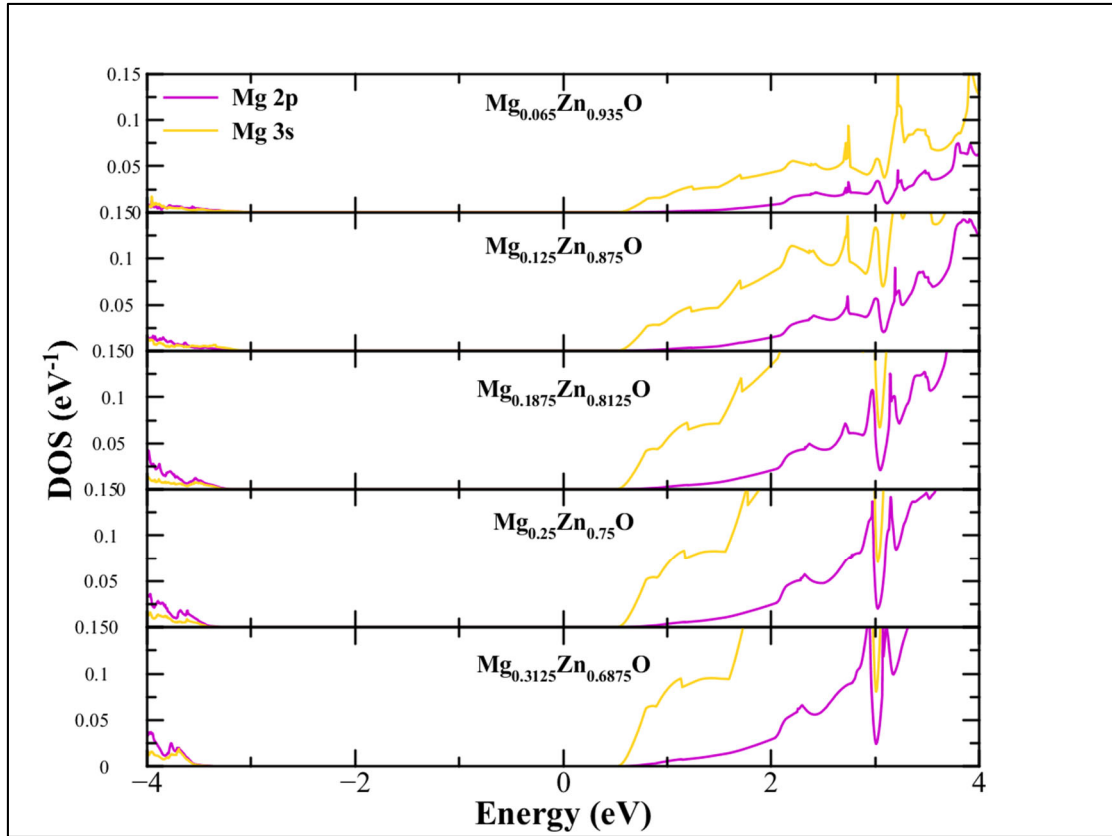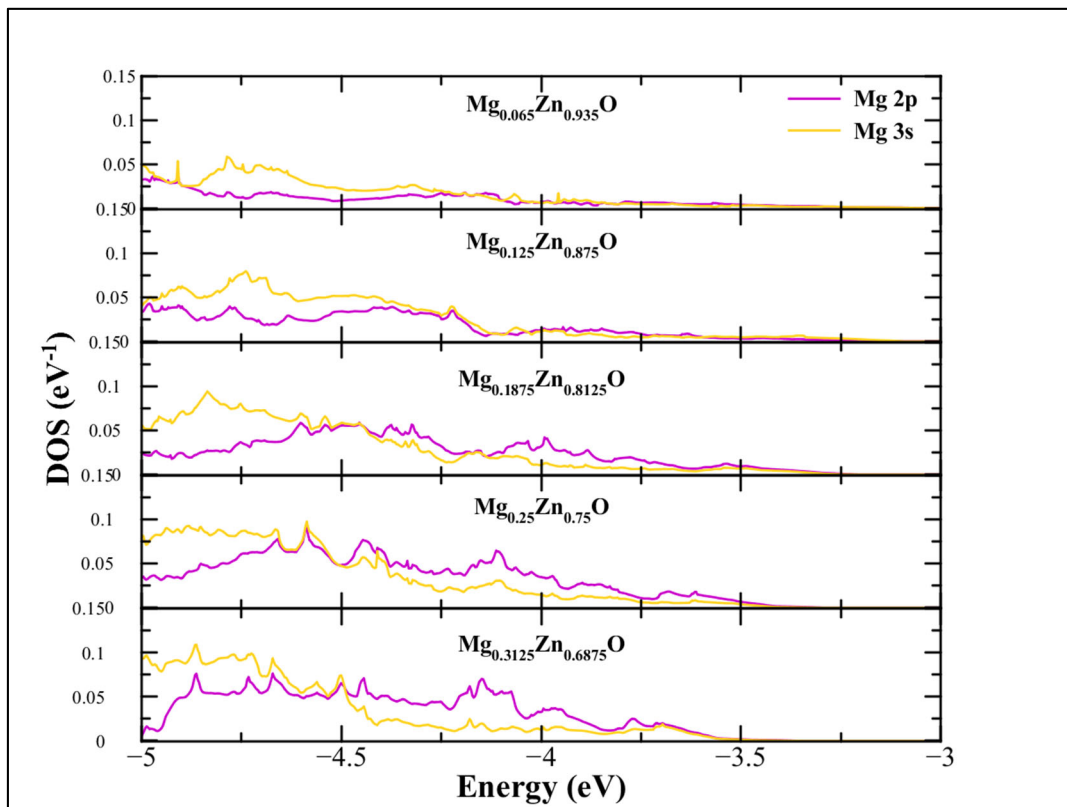The figure 5.21 shows the VBM is derived by the Mg_{2p} and Mg_{3s} states in valence band where they move to the lower energy part (-3, -3.11, -3.22, -3.31 and -3.38) eV respectively, when the Mg mole fraction increases. This is the reason the increasing band gap values of wz- $Mg_xZn_{1-x}O$.

The electron effective masses of wz- $Mg_xZn_{1-x}O$ were calculated. Table 5.1 shows the band gap energies and electron effective masses of wz- $Mg_xZn_{1-x}O$ with different Mg mole fractions. Both the band gap energies and electron effective masses increases as the Mg mole fraction increases.

Table 5.1. The band gap energies, electron effective masses and dielectric constants of $Mg_xZn_{1-x}O$ for different Mg mole fractions

Mg mole fraction x (%)	Band gap energy (eV)	Electron effective mass (m_e*)	Static dielectric constant ε_0	High-frequency dielectric constant ε_∞
0	3.35	0.383	3.06	3.14
6.25	3.48	0.390	3.01	2.80
12.5	3.59	0.396	2.97	2.70
18.75	3.70	0.404	2.92	3.23
25	3.79	0.412	2.86	3.43
31.25	3.86	0.416	2.81	3.74

The figure 5.22 shows the band gap energies of wz- $Mg_xZn_{1-x}O$ as a function of Mg mole fractions for our calculations and some of the experimental investigations. In our calculations, the band gap energies increased linearly as the Mg fractions increased, this is consistent with previous experimental investigations [67-69] as shown in figure 5.22.

The figure 5.23 shows the electron effective masses of $Mg_xZn_{1-x}O$ as a function of Mg mole fractions. As can be seen, the calculated electron effective masses of studied structures increase nearly linear with increasing Mg mole fraction, but both experimental and our results are enlarged by comparing with previous studies [43, 70].
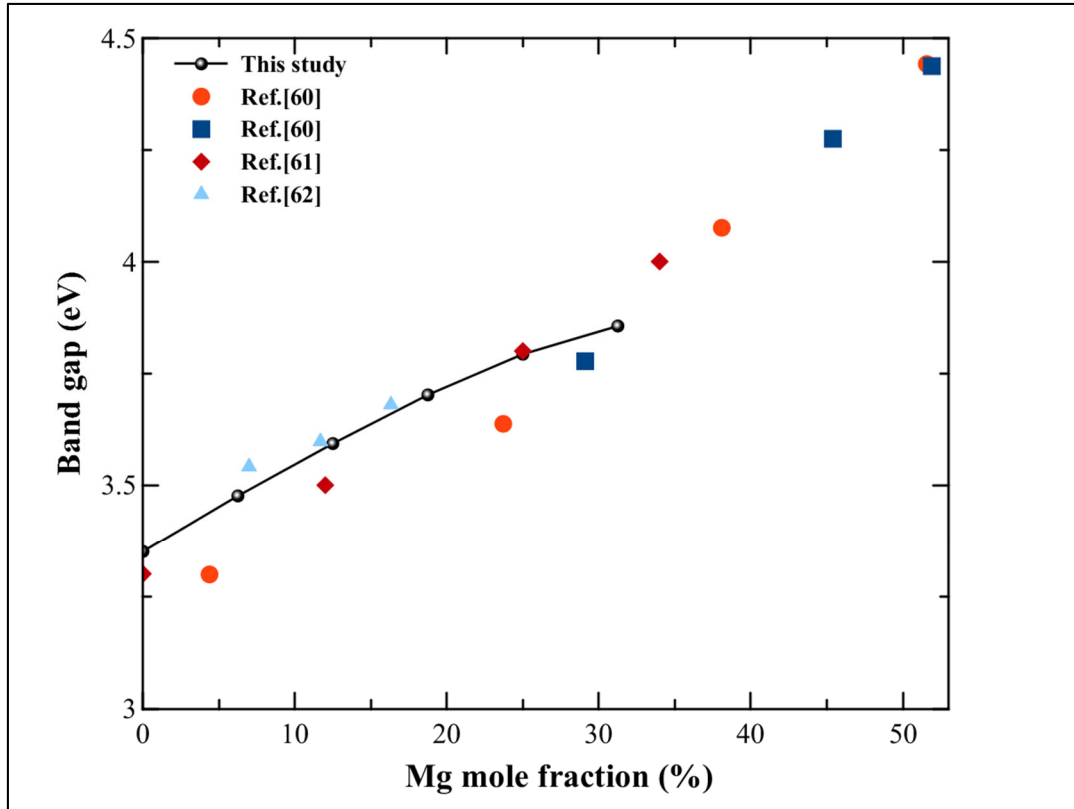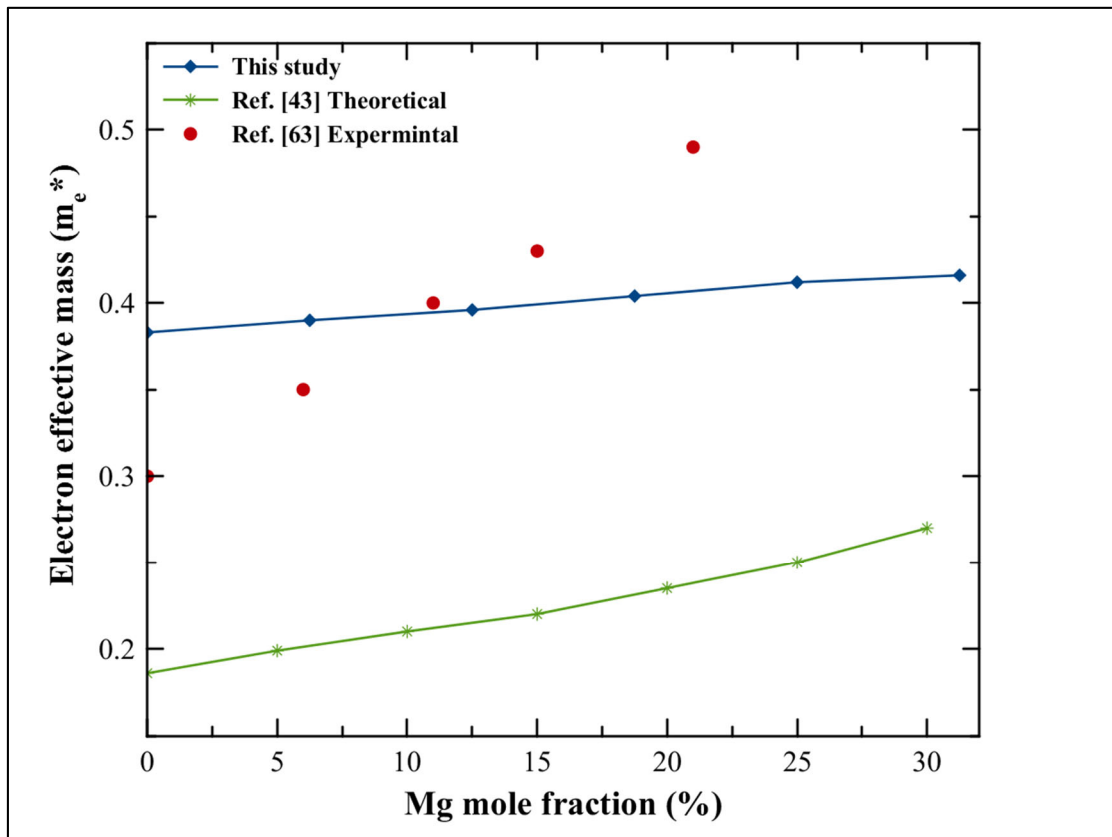
Figure 5.22. The band gap energies of wz-Mg$_x$Zn$_{1-x}$O

Figure 5.23. The electron effective masses of wz-Mg$_x$Zn$_{1-x}$O

5.3.2. Optical properties of wz- $Mg_xZn_{1-x}O$

The optical properties such as dielectric function, the refractive index, the extinction coefficient and the absorption coefficient of wz-$Mg_xZn_{1-x}O$ are calculated.

The figure shows the static dielectric constants of wz- $Mg_xZn_{1-x}O$ where they decrease as the Mg mole fraction increases. Whereas the high-frequency dielectric constants of wz-$Mg_xZn_{1-x}O$ change randomly as the Mg mole fraction increases.

The figure 5.25 shows the real part of the dielectric function for (a) light polarized perpendicular to the c axis ($E \perp c$) and (b) light polarized parallel to the c axis ($E \| c$) of ZnO and $Mg_xZn_{1-x}O$ as a function of energy, the curves and the peaks move towards the higher energies (the lower wavelengths) as the Mg mole fraction increases. As can be seen from the figure 5.26, 5.27 and 5.28 the same changes for the imaginary part of the dielectric function, the refractive index and the extinction coefficient, where the curves and the peaks move towards the higher energies (i.e. towards the lower wavelengths) as the Mg mole fraction increases.

The figure 5.29 shows the absorption spectra for (a) light polarized perpendicular to the c axis ($E \perp c$) and (b) light polarized parallel to the c axis ($E \| c$) of ZnO and $Mg_xZn_{1-x}O$ as a function to energy, the absorption edges move towards the higher energies (i.e. towards the lower wavelengths) as the Mg mole fraction increases. This corresponds to the results found in previous studies [14]. The static dielectric constant of $Mg_xZn_{1-x}O$ decreases as Mg mole fraction increases. The high frequency dielectric constants of MgZnO are found to be very close to the experimental results [71].
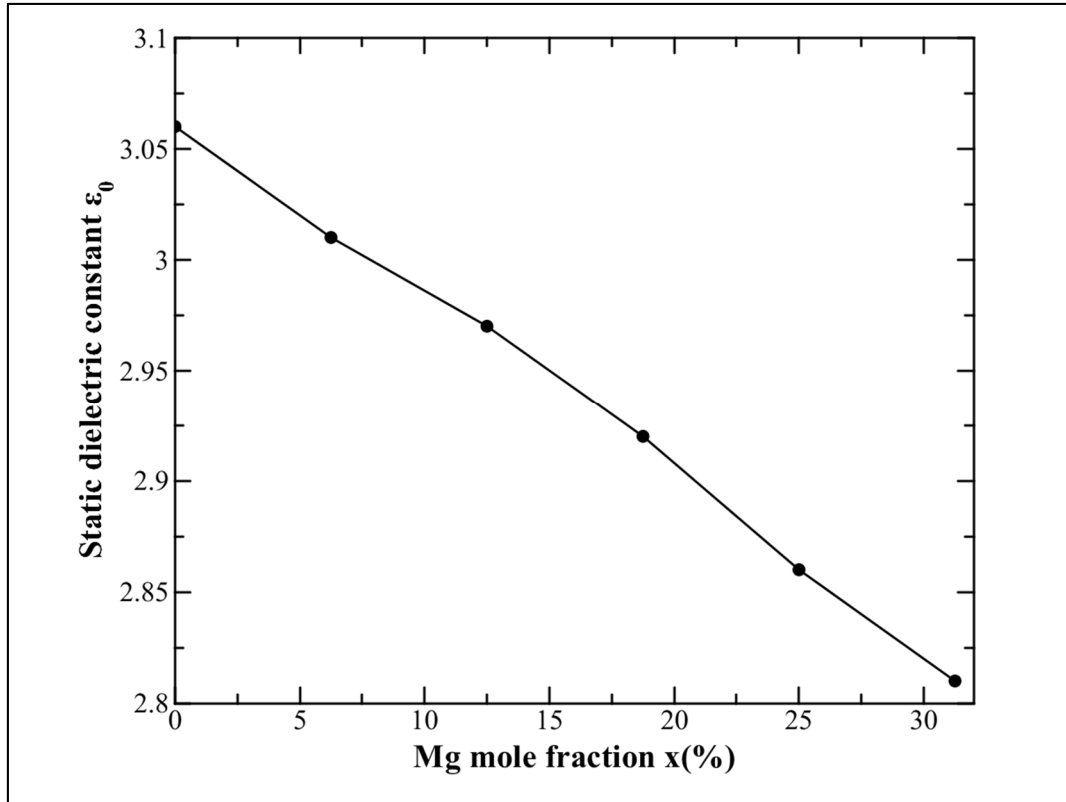
Figure 5.24. The static dielectric constant of wz- $Mg_xZn_{1-x}O$

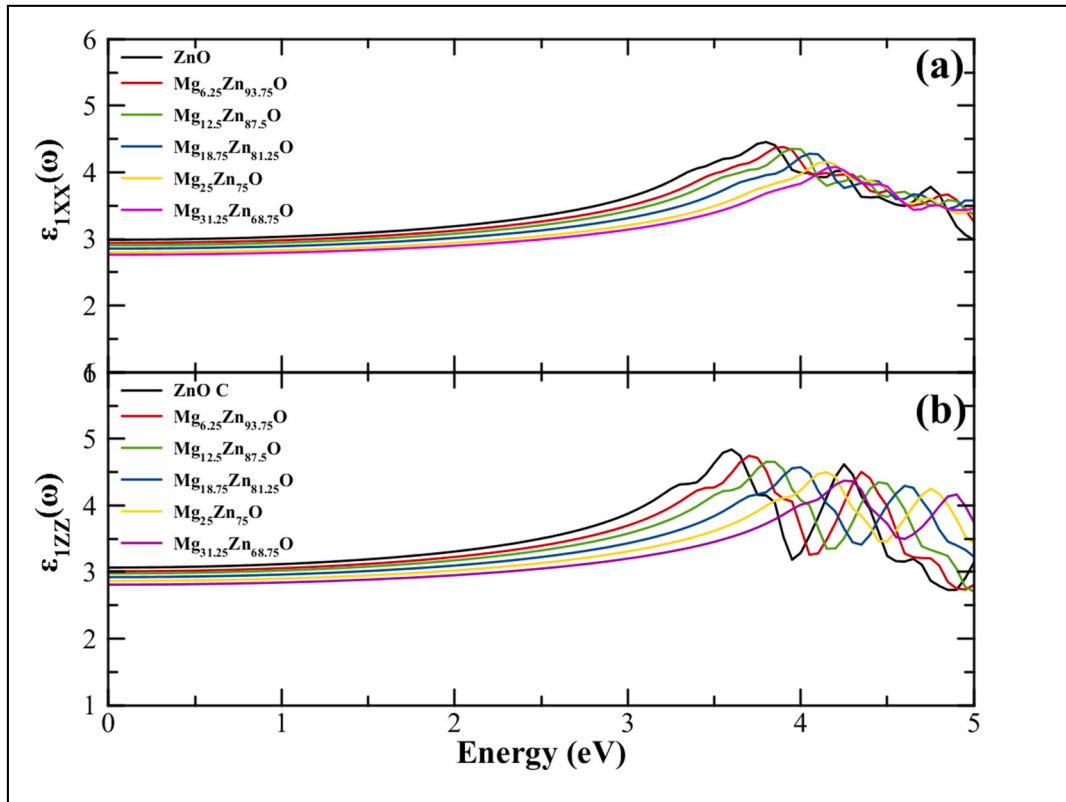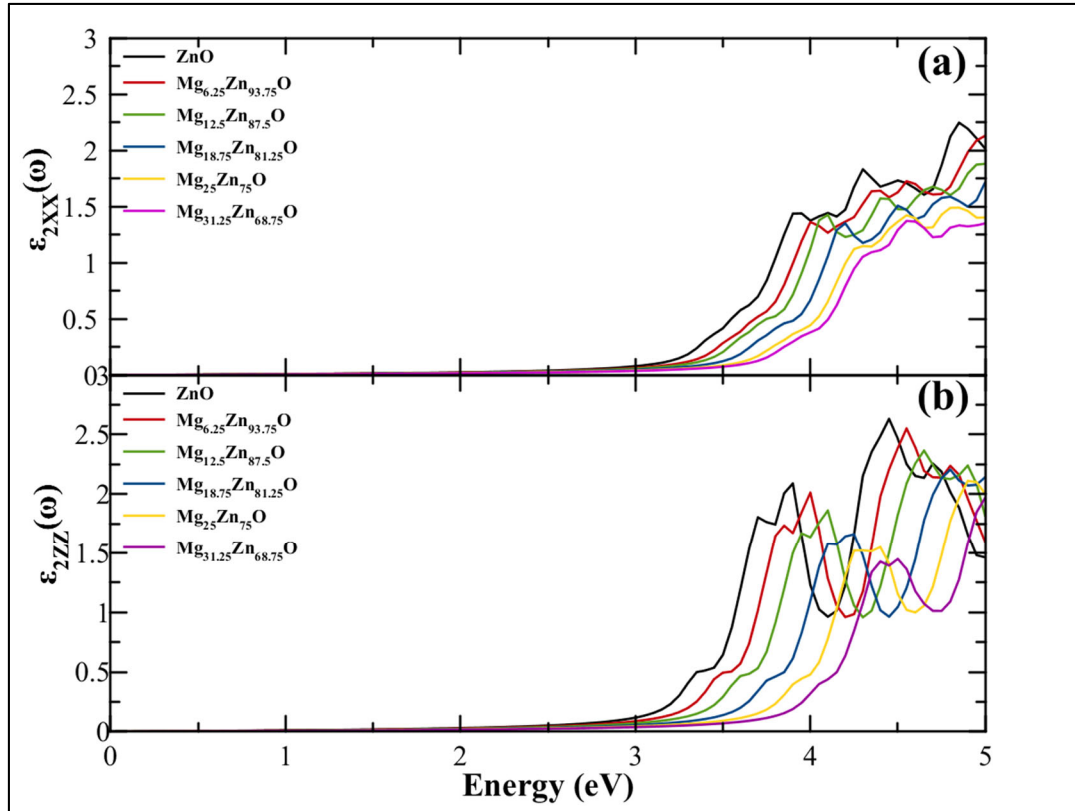Figure 5.25. The real part of the dielectric function of wz- $Mg_xZn_{1-x}O$

Figure 5.26. The imaginary part of the dielectric function of wz- $Mg_xZn_{1-x}O$
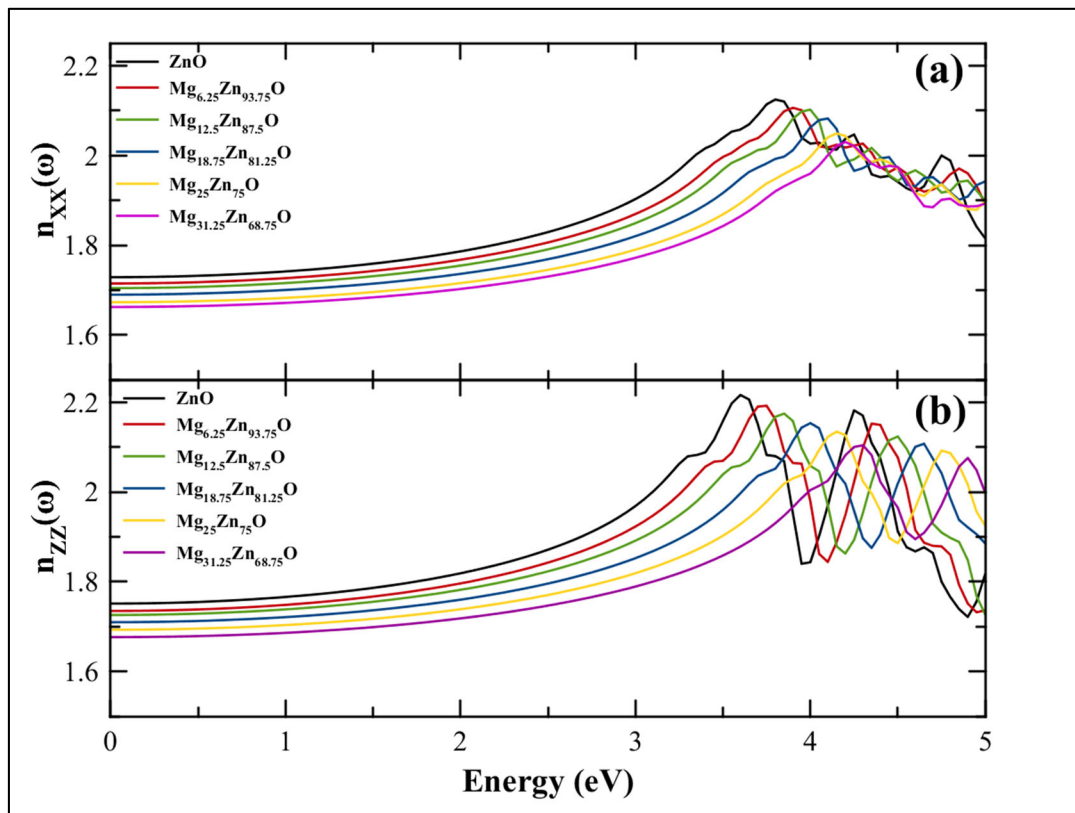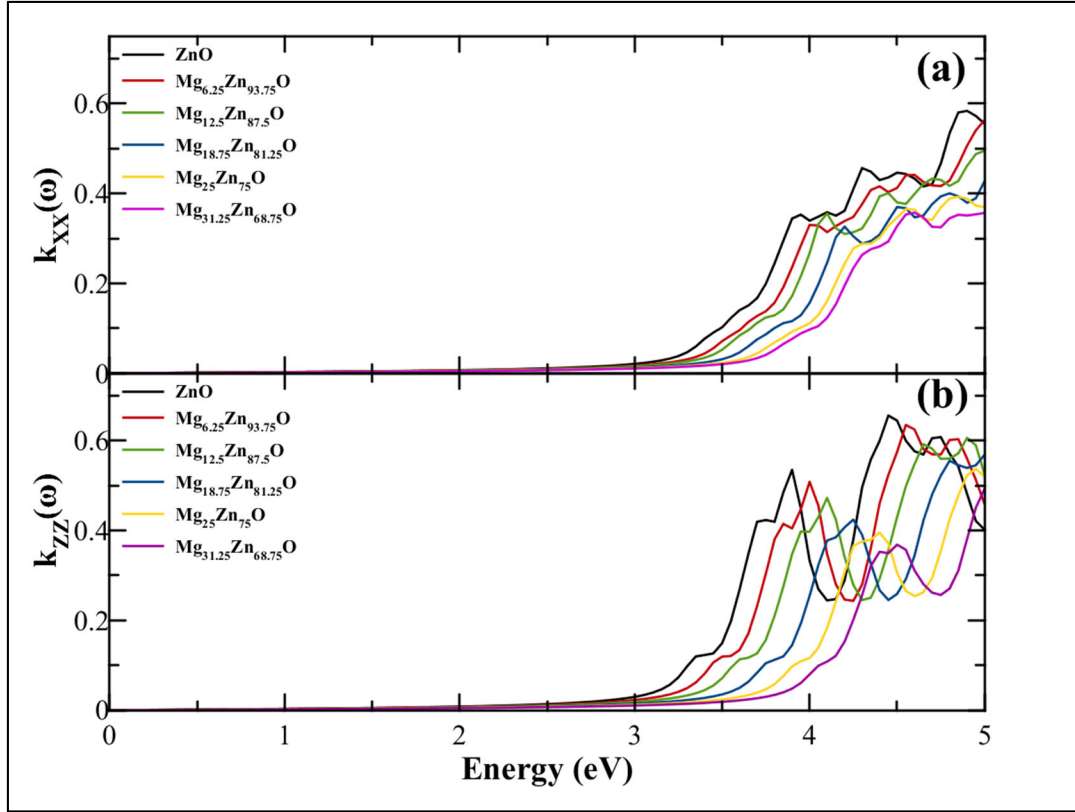

Figure 5.27. The refractive index of wz- $Mg_xZn_{1-x}O$

Figure 5.28. The extinction coefficient function of wz- $Mg_xZn_{1-x}O$
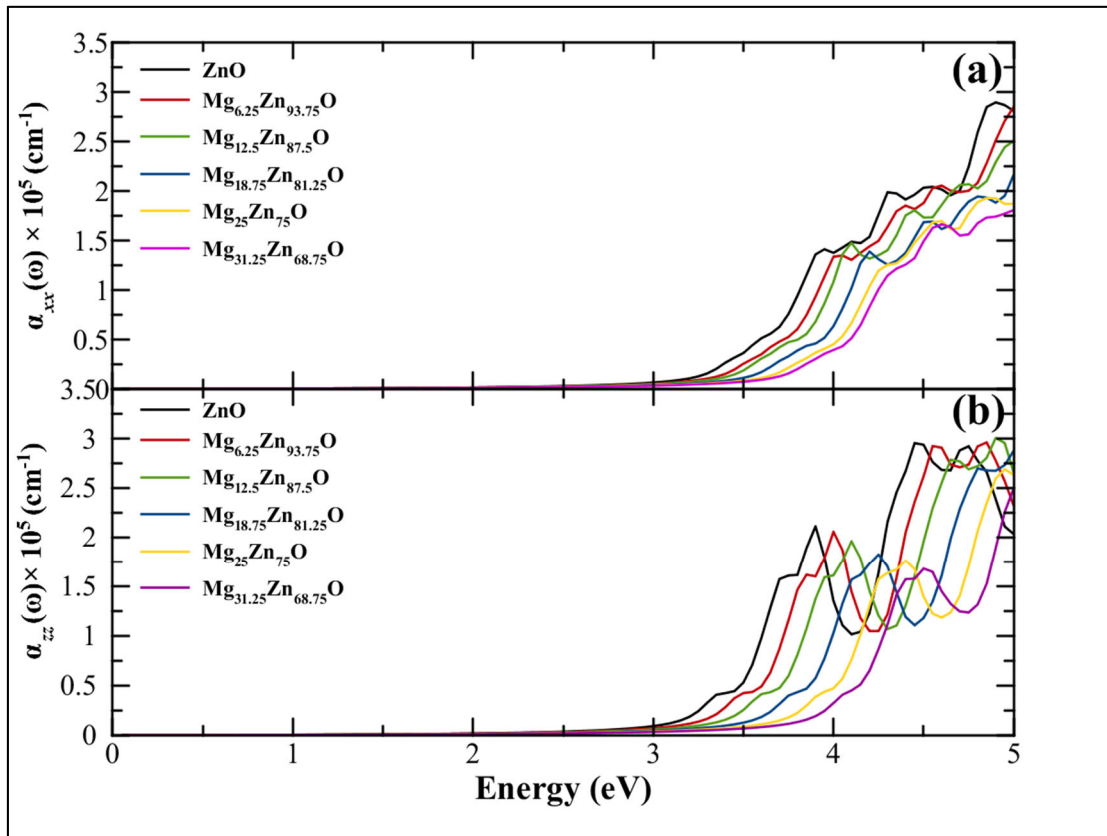

Figure 5.29. The absorption coefficient function of wz- $Mg_xZn_{1-x}O$

6. RESULTS AND DISCUSSIONS

In this study, the electronic and optical properties for wz-ZnO and wz-Mg$_x$Zn$_{1-x}$O for (x=6.25%. 12.5%. 18.75%. 25% and 31.25%) Mg mole fractions were calculated using the Atomistic Toolkit-Virtual Nano Lab (ATK-VNL) software that based on density functional theory. The calculations were performed using hybrid-generalized gradient approximation (GGA+U) where Hubbard parameters were applied on Zn$_{3d}$ orbital and O$_{2p}$ orbital to describe the on-site Coulomb corrections. In optimization calculations, experimental lattice parameters for wz-Mg$_x$Zn$_{1-x}$O crystal were used as $a = 0.32491 + 0.047$ x and $c = 0.52042 - 0.072$ x. The wz-Mg$_x$Zn$_{1-x}$O super cells were structurally optimized under an analytic potential [66]. The Hubbard parameters were U$_{O-2P}$ = 7 eV and U$_{Zn-3d}$ =10 eV. The mesh cut-off energy was 500 eV. The 6×6×5 k-points were used and a broadening of 0.1 eV is applied. Magnesium positions were randomly selected several times, where the results of all calculation were close enough.

For pure wz-ZnO, the electronic properties including the band structures, the density of state and electron effective masses were calculated. The results referred to wz-ZnO has direct wide band gap whose value corresponds to experimental values that found in the literature. The conduction band was mostly determined from the Zn$_{3d}$ electrons and O$_{2p}$ electrons whereas the valence band was mostly determined from Zn$_{4s}$ electrons. The electron effective mass of wz-ZnO was equal to 0.383 which bigger than its value in previous studies.

For pure wz-ZnO, the optical properties including the static dielectric constants, the refractive index, the extinction coefficient and the absorption spectrum were calculated. The results showed that the optical properties are anisotropic because of the difference in lattice parameters. There is no absorption for energy values below the energy gap where the electron can't be present. The a peak for the both ε_{1XX} and ε_{1YY}, that is equal to 4.46 at 3.8 eV. For ε_{1ZZ}, this peak is equal to 4.84 at 3.6 eV. the peak is equal to 2.63 at 4.45 eV for ε_{2XX} and ε_{2YY}, whereas for ε_{2ZZ} the peak is equal to 2.25 at 4.85 eV. For refractive index, there are two peaks for n_{ZZ} (2.22 and 2.18) Which corresponds to energies (3.6 and 4.25) eV. While for n_{XX}, the peaks are (2.13 and 2.05) which corresponds to energies (3.8 and 4.25) eV. They are bigger than the results found in literature. For extinction coefficient, there are two peaks for n_{ZZ} (0.54 and 0.66) which corresponds to energies (3.9

and 4.45) eV. While for n_{XX} the peaks are (0.46 and 0.59) which corresponds to energies (4.3 and 4.9) eV. They are close to the results found in the literature. For the absorption spectrum, the absorption coefficient values are ignored up to 3.35 eV, where no absorption occurs which corresponds to the band gap value where the electron is not present. There are two main peaks (21.10 and 29.51) $\times 10^6\,\text{m}^{-1}$ at (3.9 and 4.45) eV.

For wz-$Mg_xZn_{1-x}O$, the results referred to wz-MgZnO studied structures have direct wide band gaps whose values correspond to experimental values that found in the literature. The band gaps of wz-MgZnO studied structures linearly increase as Mg mole fractions increase. Both of O_{2p} state and Zn_{3d} state primarily contributed in the conduction band. In addition, the Mg_{3s} and Mg_{2p} state slightly contributed in the valence band. While the Zn_{4s} state primarily contributed to the valence band. The O_{2s}, Mg_{2p} and Mg_{3s} states also contributed in the conduction band but its contribution is smaller than Zn_{4s} state. The Mg_{2p} and Mg_{3s} state's contribution to the conduction band increases with the Mg mole fraction increases. The Zn_{3d} state contribution in the valence band become denser with the Mg mole fraction increases. The results of the partial densities states of Mg shows that the reason of the increasing the band gap values of wz-MgZnO is the VBM is derived by the Mg_{2p} and Mg_{3s} states in valence band where they move to the lower energy part when the Mg mole fraction increases. The electron effective masses of wz-MgZnO results show that the calculated electron effective masses of studied structures increase linearly with increasing Mg mole fraction, but their values are bigger than their values in previous studies.

The optical properties show that the peaks of the static dielectric constants, the refractive indexes and the extinction coefficients move towards the higher energies (i.e. towards the lower wavelengths) as the Mg mole fraction increases. The results of the absorption spectra show that the absorption edges move toward the higher energies (i.e. towards the lower wavelengths) as the Mg mole fraction increases. This corresponds to the results found in previous studies. The static dielectric constant of MgZnO decreases as Mg mole fraction increases. The high-frequency dielectric constants of MgZnO are found to be very close to the experimental results.

REFERENCES

1. Mang, A., Reimann. K., and Rübenacke, S. T. (1990). Band Gaps, Crystal-Field Splitting, Spin-Orbit Coupling, and Exciton Binding Energies in ZnO under Hydrostatic Pressure. *Solid State Communications*, 94(4), 251-254.

2. Reynolds, D. C., Look, D. C., and Jogai, B. (1996). Optically pumped ultraviolet lasing from ZnO. *Solid State Communications*, 99(12), 873-875.

3. Bagnall, D.M., Chen, Y. F., Zhu, Z., Yao.T., Koyama, S., Shen, Y., and Goto, T. (1997). Optically pumped lasing of ZnO at room temperature. *Applied Physics Letters*, 70(17), 2230-2234.

4. Paraguay, D. F., Estrada, L. W., Acosta, N. D. R., Andrade, E., and Miki-Yoshida. M. (1990). Growth, structure and optical characterization of high quality ZnO thin films obtained by spray pyrolysis. *Thin Solid Films*, 350(1-2), 192-202.

5. Florescu, D.I., Mourokh, L.G., and Pollak F.H. (2001). High spatial resolution thermal conductivity of bulk ZnO (0001). *Journal of Applied Physics*, 91(2), 890-894.

6. Kohn, W., and Sham L.J. (1965). Self-Consistent Equations Including Exchange and Correlation Effects. *American Physical Society*, 140(4A), 1133-1138.

7. Perdew, J. P., Burke, K., and Ernzerhof, M. (1996). Generalized Gradient Approximation Made Simple. *American Physical Society*, 77(18), 3865-3568.

8. Alghamdi, G. H., and Zahrani, A. Z. (2013). Bonding Formation and Orbitals Nature of ZnO Structure. *Middle East Journal of Scientific Research*, 13(9), 1144-1149.

9. Wang, V., Deming, M., Wanli, J., and Weiili, J. (2012). Structural and Electronic Properties of Hexagonal ZnO: A Hybrid Functional Study. *Solid State Communications*, 152(22), 45-48.

10. Yaakob, M. K., Hussin, N. H., Taib, M. F. M., Kudin, T. I. T., Hassan, O. H., Ali, A. M. M., and Yahya. M. Z. A. (2014). First Principles LDA+U Calculations for ZnO Materials. *Integrated Ferroelectrics*, 155(1), 15-22.

11. Walsh, A., Juarez, L. F, Silva, Da., and Huaiwei. S.U. (2008). Theoretical Description of Carrier Mediated Magnetism in Cobalt Doped ZnO. *Physical Review Letters*, 100(25), 6401-6404.

12. Xinguo. Ma, Ying. Wu, Yanhui.Lv and Yongfa Zhu. (2013). Correlation Effects on Lattice Relaxation and Electronic Structure of ZnO within the GGA+U Formalism. *The Journal of Physical Chemistry C*, 117(49), 26029-26039.

13. Gao, J., Zhao, G. J., Liang, X. X., and Song, T. L. (2015). First-principles Study of Structural Properties of $Mg_xZn_{1-x}O$ ternary alloys. *Journal of Physics: Conference Series*, 574(1).

14. Li, Na., B, Jian-She, L., and Qing, J. (2011). Optical and Electronic Properties of Wurtzite Structure $Zn_{1-x}Mg_xO$ Alloys. *Chinese Physical Society,* 28(11), 1011-1014.

15. Ferblantier, G., Mailly, F., Al-Asmar, R., Foucaran, A., and Pascal-Delannoy, F. (2005). Deposition of zinc oxide thin films for application in bulk acoustic wave resonator. *Sensors and Actuators A:Physical*, 122(2, 184-188.

16. Özgür, Ü., Alivov, Ya. I., Liu, C., Teke, A., Reshchikov, M. A., Doğan, S., Avrutin,V., Cho, S. J., and Morkoç, H. (2005). A comprehensive review of ZnO materials and devices. *Journal of Applied Physics*. 98(4), 301-305.

17. Jin, C. H. (2003). *Growth and characterization of ZnO and ZnO-based Alloys-MgxZn1-xO and MnxZn1-xO.* PhD thesis, North Carolina state university, Department of materials science and Engineering, Raleigh.

18. Hughes, W. (2006). *Synthesis and characterization of ZnO for piezoelectric applications*. PhD thesis, Georgia Institute of Technology USA, School of Materials Science and Engineering, Atlanta.

19. Ginley, D. S and Perkins, J. D. (2011). Transparent conductors. Boston: Handbook of Transparent Conductors Springer, 1-25.

20. Meyer, B. K. (2011). ZnO: crystal structures, structural phases, transition pressures. In *New Data and Updates for IV-IV, III-V, II-VI and I-VII Compounds, their Mixed Crystals and Diluted Magnetic Semiconductors*. Springer, Berlin: Heidelberg, 565-565.

21. Morkoç, H., and Özgür, Ü. (2008). *Zinc oxide: fundamentals, materials and device technology*. Springer, Berlin: Heidelberg. John Wiley & Sons, 2-5.

22. West, A. R. (1999). *Basic solid state chemistry.* Springer, Berlin: Heidelberg. John Wiley & Sons Inc.

23. Madelung, O. (2012). *Semiconductors: data handbook.* 3. Edition. Media Springer-Verlag Berlin Heidelberg New York, 194-200.

24. Ivanov, I., and Pollmann, J. (1981). Electronic structure of ideal and relaxed surfaces of ZnO: A prototype ionic wurtzite semiconductor and its surface properties. *Physical Review B*, 24(12), 7275-7287.

25. Göpel, W., Pollmann, J., Ivanov, I., and Reihl, B. (1982). Angle-resolved photoemission from polar and nonpolar zinc oxide surfaces. *Physical Review B*, 26 (6), 3144-3150.

26. Uthirakumar. A.P. (2011). Fabrication of ZnO Based Dye Sensitized Solar Cells. In Solar Cells-Dye-Sensitized Devices. *Nanoscale Research Letters*, **7**(6), 166-172.

27. Gopal, P., and Spaldin, N. A. (2006). Polarization, piezoelectric constants, and elastic constants of ZnO, MgO, and CdO. *Journal of Electronic Materials, 35*(4), 538-542.

28. Gsiea, A. M., Goss, J. P., Briddon, P. R., Ramadan, A. L., Etmim, K. M., Khaled, A., Marghani, S., (2014). Native Point Defects in ZnO. *International Journal of Materials and Metallurgical Engineering*, 8(1), 127-132.

29. Look, D. C., Hemsky, J. W., and Sizelove, J. R. (1999). Residual Native Shallow Donor in ZnO. *Physical Review Letters*, 82(12), 52-64.

30. Kang, H. S., Kang, J. S., Kim, J. W., and Lee, S. Y. (2004). Annealing effect on the property of ultraviolet and green emissions of ZnO thin films. *Journal of Applied Physics*, 95(3), 46-48.

31. Park, C. H., S. B., Zhang, S. B., and Huai Wei, S. (2002). Origin of p-type doping difficulty in ZnO: The impurity perspective. *Physical Review B*, 66(7), 202-208.

32. Hu, J., and Pan, B. C. (2008). Electronic structures of defects in ZnO: Hybrid density functional studies. *The Journal of Chemical Physics*, 129(8), 61-68.

33. Rodnyi, P. A., and Khodyuk, I. V. (2011). Optical and Luminescence Properties of Zinc Oxide. *Optics and Spectroscopy*, 111(5), 776-785.

34. Gon, A. R., and Syassenk, K. (1998). Optical Properties of Semiconductors under Pressure. *Semiconductors and Semimetals*, 54(178). 247-425.

35. Zhang, X. T., Liu, Y. C., Zhang, L. G., Zhang, J. Y., Lu, Y. M., Shen, D. Z., Xu, W., Zhong, G.Z., Fan, X. W., and Kong, X.G. (2002). Structure and Optically Pumped Lasing from Nanocrystalline ZnO Thin Films Prepared by Thermal Oxidation of ZnS Thin Films. *Journal of Applied Physics*, 92(6), 93-98.

36. Zhai, B., Yang. L., Lan Ma, Q., and Huang, Y. M. (2015). First-Principles Calculations of Band Structures and Optical Properties of Hexagonal ZnO by Using meta–GGA in the Framework of Density Functional Theory. *Optoelectronic Materials*, 1(5), 13-17.

37. Hussain, S. (2008). *Investigation of Structural and Optical Properties of Nanocrystalline ZnO.* Master Thesis, Linköping's University. The Department of Physics, Chemistry and Biology. Linköping, Sweden, 13-14.

38. Wu, X., Lee, J., Varshney, V., Wohlwend, J. L., Roy, A. K., and Luo, T. (2016). Thermal conductivity of wurtzite zinc-oxide from first-principles lattice dynamics–a comparative study with gallium nitride. *Scientific reports*, 6, 22504

39. Schleife, A., Fuchs, F., Furthmüller, J., and Bechstedt, F. (2006). First-principles study of ground- and excited-state properties of MgO, ZnO and CdO polymorphs. *Physical Review B*, 73(14), 2121-21214.

40. Hou, Y., Mei, Z., and Du, X. (2014). Semiconductor ultraviolet photodetectors based on ZnO and MgxZn$1-x$O. *Journal of Physics D: Applied Physics*, 47(25), 283001-28325.

41. Liping, Q., Changchun, C., Yintang, Y., Xinhai, Y., and Chunlei, S. (2014). Strain effects on band structure of wurtzite ZnO: a GGA+ U study. *Journal of Semiconductors,* 35(7), 41-45

42. Ashrafi, A. A., and Segawa, Y. (2005). Determination of Mg composition in MgZO alloy: Validity of Vegard's law. *Journal of Vacuum Science and Technology B:*

Microelectronics and Nanometer Structures Processing, Measurement, and Phenomena, 23(5), 2030-2033.

43. Franz, C., Giar, M., Heinemann, M., Czerner, M., and Heiliger, C. (2012). Band Structure and Effective Masses of Zn1-xMgx O. *Materials Research Society,* 1494, 57-63.

44. Ohtomo, A., Kawasaki, M., Koida, T., Masubuchi, K., Koinuma, H., Sakurai, Y., Yoshida. Y., Yasuda. T and Segawa, Y. (1998). Mg x Zn 1− x O as a II–VI widegap semiconductor alloy. *Applied Physics Letters,* 72(19), 2466-2468

45. Chen, J., Shen, W. Z., Chen, N. B., Qiu, D. J., and Wu, H. Z. (2003). The study of composition non-uniformity in ternary $Mg_xZn_{1-x}O$ thin films. *Journal of Physics: Condensed Matter,* 15(30), L475.

46. Wu, C., Lu, Y., Shen, D. and Fan, X. (2010). Effect of Mg content on the structural and optical properties of Mg x Zn 1− x O alloys. *Chinese Science Bulletin,* 55(1), 90-93.

47. Aoumeur-Benkabou, F. Z., Ameri, M., Kadoun, A. and Benkabou, K. (2012). Theoretical Study on the Origins of the Gap Bowing in MgxZn1–xO Alloys. *Modeling and Numerical Simulation of Material Science,* 2(03), 60-66.

48. Cohen, D. J., Ruthe, K. C., & Barnett, S. A. (2004). Transparent conducting Zn_{1-x} Mg_x O:(Al, In) thin films. *Journal of Applied Physics,* 96(1), 459-467.

49. Zeng, Y. J., Ye, Z. Z., Xu, W. Z., Li, D. Y., Lu, J. G., Zhu, L. P. and Zhao, B. H. (2006). Dopant source choice for formation of p-type ZnO: Li acceptor. *Applied Physics Letters,* 88(6), 062107.

50. Janotti, A., and Van de Walle, C. G. (2007). Absolute deformation potentials and band alignment of wurtzite ZnO, MgO, and CdO. *Physical Review B,* 75(12), 121201.

51. Tampo, H., Shibata, H., Maejima, K., Yamada, A., Matsubara, K., Fons, P., Kashiwayal. S, Nikil, S, Chiba, Y. and Kanie, H. (2008). Polarization-induced two-dimensional electron gases in ZnMgO/ZnO heterostructures. *Applied Physics Letters,* 93(20), 202104-202123.

52. Bartlett, R. J., and Stanton, J. F. (1994). Applications of post-hartree-fock methods: A tutorial. *Reviews in Computational Chemistry,* 65-169.

53. Bucko, T., Hafner, J., Lebegue, S., and Angyán, J. G. (2010). Improved description of the structure of molecular and layered crystals: ab initio DFT calculations with van der Waals corrections. *The Journal of Physical Chemistry A,* 114(43), 11814-11824.

54. Runge, E., and Gross, E. K. (1984). Density-functional theory for time-dependent systems. *Physical Review Letters,* 52(12), 997.

55. Woolley, R. G., and Sutcliffe, B. T. (1977). Molecular structure and the born-Oppenheimer approximation. *Chemical Physics Letters,* 45(2), 393-398.

56. Kryachko, E. S. (1980). Hohenberg-Kohn theorem. *International Journal of Quantum Chemistry,* 18(4), 1029-1035.

57. Castro, A., Marques, M. A., and Rubio, A. (2004). Propagators for the time-dependent Kohn–Sham equations. *The Journal of Chemical Physics*, 121(8), 3425-3433.

58. Yabana, K., and Bertsch, G. F. (1996). Time-dependent local-density approximation in real time. *Physical Review B,* 54(7), 4484.

59. Himmetoglu, B., Floris, A., De Gironcoli, S., and Cococcioni, M. (2014). Hubbard-corrected DFT energy functionals: The LDA+ U description of correlated systems. *International Journal of Quantum Chemistry,* 114(1), 14-49.

60. Kümmel, S., and Kronik, L. (2008). Orbital-dependent density functionals: Theory and applications. *Reviews of Modern Physics,* 80(1), 3.

61. Chivian, D., Robertson, T., Bonneau, R., and Baker, D. (2003). Ab initio methods. *Structural Bioinformatics,* 44, 547-557.

62. Cohen, M. L., Schlüter, M., Chelikowsky, J. R., and Louie, S. G. (1975). Self-consistent pseudopotential method for localized configurations: Molecules. *Physical Review B,* 12(12), 5575.

63. Chelikowsky, J. R., and Louie, S. G. (1984). First-principles linear combination of atomic orbitals method for the cohesive and structural properties of solids: Application to diamond. *Physical Review B,* 29(6), 3470.

64. Sheetz, R. M., Ponomareva, I., Richter, E., Andriotis, A. N., and Menon, M. (2009). Defect-induced optical absorption in the visible range in ZnO nanowires. *Physical Review B,* 80(19), 195314.

65. Bond, W. L. (1965). Measurement of the refractive indices of several crystals. *Journal of Applied Physics,* 36(5), 1674-1677.

66. Pedone, A., Malavasi, G., Menziani, M. C., Cormack, A. N., and Segre, U. (2006). A new self-consistent empirical interatomic potential model for oxides, silicates, and silica-based glasses. *The Journal of Physical Chemistry B,* 110(24), 11780-11795.

67. Kamada, Y., Kawaharamura, T., Nishinaka, H., and Fujita, S. (2006). Linear-source ultrasonic spray chemical vapor deposition method for fabrication of ZnMgO films and ultraviolet photodetectors. *Japanese Journal of Applied Physics,* 45(8L), L857.

68. Takagi, T., Tanaka, H., Fujita, S., and Fujita, S. (2003). Molecular Beam Epitaxy of High Magnesium Content Single-Phase Wurzite MgxZn1-xO Alloys (x≃ 0.5) and Their Application to Solar-Blind Region Photodetectors. *Japanese Journal of Applied Physics,* 42(4B), L401.

69. Sheng, H., Emanetoglu, N. W., Muthukumar, S., Feng, S., and Lu, Y. (2002). Nonalloyed Al ohmic contacts to Mg x Zn 1− x O. *Journal of Electronic Materials,* 31(7), 811-814.

70. Lu, J. G., Fujita, S., Kawaharamura, T., Nishinaka, H., Kamada, Y., and Ohshima, T. (2006). Carrier concentration induced band-gap shift in Al-doped $Zn1-x$ Mg_xO thin films. *Applied Physics Letters,* 89(26), 262107.

71. Bundesmann, C., Rahm, A., Lorenz, M., Grundmann, M., and Schubert, M. (2006). Infrared optical properties of Mg_x Zn_1-x O thin films ($0 \leqslant x \leqslant 1$): Long-wavelength optical phonons and dielectric constants. *Journal of Applied Physics,* 99(11), 113504.

Curriculum Vitae

Personal Information

Surname, name	: Ibrahem, Rokaia
Nationality	: Syrian
Birth date and place	: 6/1/1990, Damascus
Marital status	: Single
Mobile	: 0 (534) 910 48 85
Mail	: ribrahem@gmail.com
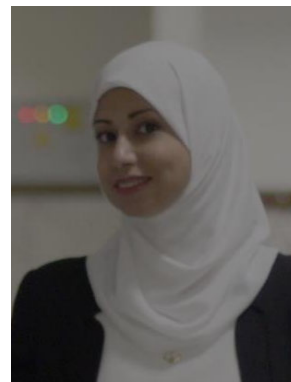
Education

Degree	School/Program	Date of graduation
Master	Gazi University/ Physics	Continuing
Undergraduate	Damascus University/Physics	2012
High school	Hajira secondary girls school	2008

Languages

English, Turkish and Arabic.

Publications

1. Ibrahem, R., Narin. P., Lisesivdin. B. and Ozbay, E. (2017). *Optimized Ab Initio Studies on Electronic Structure of Wurtzite MgZnO*. Turkish physical 33rd International Physics Congress. Bodrum.

2. Ibrahem, R., Narin. P., Lisesivdin. B. and Ozbay, E. (2018). *Frist-principles calculation of Optical properties of Magnesium Zinc Oxide*. 20th National Optical, Electro-Optics and Photonics Workshop (PHOTONICS 2018). Ankara.

Hobbies

Reading books and novels.

GAZİ GELECEKTİR...